表　JCOG と SNNS 研究会による二つの多施設共同研究の比較

	JCOG	SNNS 研究会
primary endpoint	偽陰性割合(術中迅速病理診断)	転移検出感度
対象	sT I N 0	cT I-2 N 0
トレーサー	ICG	^{99m}Tc スズコロイド 1% isosulfan blue
同定方法	術中 pick up(時間規定あり)	術野サンプリングしたものに加えて切除標本での検索
転移検索方法	術中迅速病理診断	術中迅速診断を原則とするが最終的転移診断は永久標本判定
登録方法	術中登録	術前日までの前登録
参加施設	30 施設(手技慣れ各施設 5 例)	30 例以上の経験をもつ 12 施設
予定登録数	1,550 例	500 例

行われている(表).

JCOG 胃がん外科グループによる多施設共同研究「早期胃癌におけるセンチネルリンパ節生検の妥当性に関する研究(JCOG 0302)」(UMIN-CTR 試験 ID：C 000000059)は，早期胃癌患者に対して，indocyanine green (ICG)を用いて同定された green node(GN)を SN とみなし，GN の術中迅速病理診断でリンパ節転移が陰性の場合にリンパ節郭清を行わないことが妥当であるかどうかを評価することを目的とする．primary endpoint は偽陰性割合(GN 迅速病理診断転移陰性例/組織学的リンパ節転移陽性例)である．

本試験は，胃癌における SN 生検の妥当性を評価する試験であり，同意の得られた内視鏡的切除の対象とならない早期胃癌患者の術中に登録を行う．腫瘍部位の漿膜側から色素(ICG)を注入し GN を同定する．これを摘出して迅速病理診断に提出し，通常のリンパ節郭清を伴う胃切除を『胃癌治療ガイドライン』[13]に沿って施行する．後日，リンパ節の固定標本の病理結果と GN の結果を比較検討する(図).

本試験の結果により SN 生検によってリンパ節転移の有無を診断することが妥当であると判

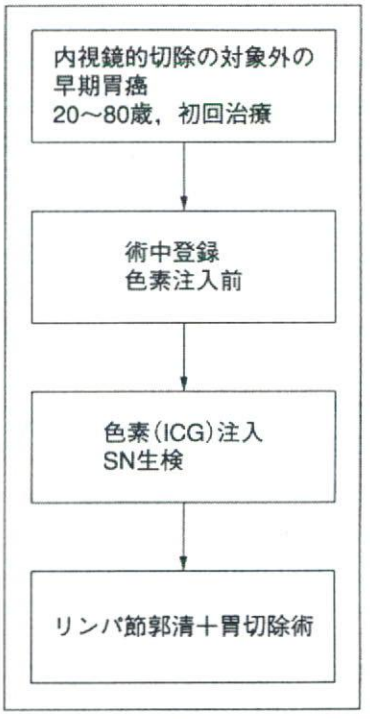

図　JCOG 0302 の概要

断された場合，SN 転移陰性の早期胃癌患者に対しては第Ⅲ相試験が行われることなく，胃局所切除術などのリンパ節郭清を省略した術式が標準治療となると予想される．現時点での臨床応用が妥当であるかどうかを評価する臨床試験であり，SN 転移診断は術中診断に限定されている．たとえば，術中の迅速病理診断で転移な

しとされたGNの術後検索で転移を認めた場合，SN conceptとしては問題ないのだが，本試験では偽陰性と扱われる．なお，本試験のベースとなった筆者らのpilot studyでは多切片での転移検索を行っていたが[1]，多施設共同研究であるために最大割面1切片のHE染色のみでの検索という制約が加わっている．また，SN生検の手技慣れ期間が施設当り5例と設定されているが，後述のSNNS研究会によるアンケート結果からすれば，ラーニングカーブが少なく見積もられている．

Ⅲ．JCOGとSNNS研究会による多施設共同研究の相違点

この項のポイント

- JCOGとSNNS研究会による多施設共同研究には留意すべき相違点があり，結果が公表された際には，両者の相違点をふまえて解釈する必要がある．

JCOG 0302は現時点での臨床応用が妥当であるかどうかを評価する臨床研究であるため，SN conceptの妥当性のみならず，術中迅速病理診断および手技慣れ期間(ラーニングカーブ)の問題が包含されている点に留意すべきである．すなわち，肯定的な結果が得られた場合は，その時点で臨床応用の根拠となるが，否定的な結果であった場合，SN concept自体の問題なのか，最大1割面の術中迅速病理診断による転移検索法の問題なのか，ラーニングカーブの問題なのかという疑問が残ることになる．

SNNS研究会標準手技プロトコール作成委員会による多施設共同研究「胃癌におけるセンチネルリンパ節を指標としたリンパ節転移診断に関する臨床試験」は，早期胃癌に加えて一部の進行胃癌(cT 2)を対象とし，^{99m}Tcスズコロイドと1% isosulfan blueを内視鏡を用いて病巣周囲粘膜下層に原則4カ所注入するもので，primary endpointは転移検出感度(リンパ節郭清の結果で所属リンパ節に少なくとも1個以上のリンパ節に転移が認められた症例のうちSNに転移を有した症例の割合)である．

JCOG 0302との相違点として，トレーサー併用であること，術野サンプリングしたものに加えて切除標本での検索を許容すること，術中迅速病理診断を原則とするが最終的リンパ節転移診断は永久標本での判定であること，30例以上の経験をもつ12施設に限定したものであること，などがあげられる(表)．SNNS研究会が行ったアンケート調査から，ラーニングカーブとして30例を要するとみられたことをふまえ，手技慣れを前提にSN conceptが胃癌においても成立するかをみることを主眼としており，術中迅速病理診断およびラーニングカーブの影響を受けにくいように設定されている．しかしながら，SN同定およびこれを指標としたリンパ節転移診断が胃切除前に限定されていないため，肯定的な結果が得られても，その結果をもって術中診断による臨床応用が可能とはいえず，臨床応用のためには別ステップを要することになる．

おわりに

胃癌におけるSN conceptは，多施設共同研究によりその妥当性が検証されている段階であり，日常診療として安易に臨床応用すべき状況にはない．JCOGとSNNS研究会による二つの多施設共同研究は，SN conceptの胃癌への応用が可能かどうかを見極める重要な試験である．その結果が待たれるが，両研究には留意すべき相違点があり，結果が公表された際には，両者の相違点をふまえて解釈する必要がある．

文　献

1) Hiratsuka, M., Miyashiro, I., Ishikawa, O., et al.：Application of sentinel node biopsy to gastric cancer surgery. Surgery　129；335-340, 2001
2) Kitagawa, Y., Fujii, H., Mukai, M., et al.：The role of the sentinel lymph node in gastrointestinal cancer. Surg. Clin. North Am.　80；1799-1809, 2000
3) Kitagawa, Y., Fujii, H., Mukai, M., et al.：Radio-guided sentinel node detection for gastric cancer. Br. J. Surg.　89；604-608, 2002
4) Ichikura, T., Morita, D., Uchida, T., et al.：Sentiel node concept in gastric carcinoma. World J. Surg.　26；318-322, 2002
5) 市倉　隆，小野　聡，望月英隆：Sentinel node navigation surgery—消化器癌への応用の可能性．医学のあゆみ　205；586-590, 2003
6) Morton, D. L., Wen, D. R., Wong, J. H., et al.：Technical details of intraoperative lymphatic mapping for early stage melanoma. Arch. Surg.　127；392-399, 1992
7) Krag, D. N., Weaver, D. L., Alex, J. C., et al.：Surgical resection and radio-localization of the sentinel node in breast cancer using a gamma probe. Surg. Oncol.　2；335-340, 1993
8) Giuliano, A. E., Kirgan, D. M., Guenther, J. M., et al.：Lymphatic mapping and sentinel lymphadenectomy for breast cancer. Ann. Surg.　220；391-401, 1994
9) 宮代　勲，平塚正弘，石川　治，他：胃癌における sentinel node concept の現状．外科　68；1688-1693, 2006
10) Nieweg, O. E., Tanis, P. J. and Kroon, B. B. R.：The definition of a sentinel node. Ann. Surg. Oncol.　8；538-541, 2001
11) 平塚正弘，宮代　勲：センチネルリンパ節からみた胃癌対策．Front. Gastroenterol.　10；242-247, 2005
12) 宮代　勲，平塚正弘，今岡真義：センチネルリンパ節の概念は消化器癌の外科治療を変えるか？変えるとする立場から．Front. Gastroenterol.　6；116-120, 2001
13) 日本胃癌学会編：胃癌治療ガイドライン(医師用)2004年4月改訂(第2版)．金原出版，東京，2004
14) Cimmino, V. M., Brown, A. C., Szocik, J. F., et al.：Allergic reactions to isosulfan blue during sentinel node biopsy—a common event. Surgery　130；439-442, 2001
15) 高山　敏，古賀和久，大浦　憲，他：Indocyanine green のリンパ系着色剤としての有用性．応用薬理　19；603-614, 1980
16) 三輪晃一，木南伸一，鯵坂秀行，他：リンパ区域郭清を伴う早期胃がんの機能温存縮小手術．日外会誌　106；280-285, 2005
17) 平塚正弘，宮代　勲，石川　治：胃癌—色素法による成績．北島政樹，久保敦司編：Sentinel Node Navigation—癌治療への新しい展開．171-176，金原出版，東京，2002

Summary

Outline of the Japan Clinical Oncology Group Trial—Evaluation of Feasibility and Accuracy of Diagnosis Using Sentinel Node Biopsy in Early Gastric Cancer (JCOG 0302)

Isao Miyashiro*, Masahiro Hiratsuka**, Takeshi Sano*3, Mitsuru Sasako*3, Kenichi Yoshimura*4, and Gastric Cancer Surgical Study Group, Japan Clinical Oncology Group

Multi-institutional prospective clinical trials to evaluate feasibility and accuracy of diagnosis using sentinel node biopsy in early gastric cancer are essential for clinical application of this technique. Two clinical trials, the Japan Clinical Oncology Group trial (JCOG 0302) and the Japanese Society for Sentinel Node Navigation Surgery trial, are ongoing in Japan. Several noteworthy differences between these two trials are noted.

Key words : sentinel node, gastric cancer, multi-institutional prospective clinical trial, less-invasive

**Department of Surgery, Osaka Medical Center for Cancer and Cardiovascular Diseases, 1-3-3 Nakamichi, Higashinari-ku, Osaka 537-8511, Japan*

***Department of Surgery, Itami Municipal Hospital*

*3*Department of Surgery, National Cancer Center Hospital*

*4*JCOG Data Center, National Cancer Center*

Identification of a predictive gene expression signature of cervical lymph node metastasis in oral squamous cell carcinoma

Su Tien Nguyen,[1,3] Shogo Hasegawa,[2] Hitoshi Tsuda,[4] Hirofumi Tomioka,[2] Masaru Ushijima,[5] Masaki Noda,[3,7] Ken Omura[2,3] and Yoshio Miki[1,3,6,8]

[1]Department of Molecular Genetics, Medical Research Institute, [2]Oral and Maxillofacial Surgery, Department of Oral Restitution, Division of Oral Health Sciences, Graduate School and [3]21st Century Center of Excellent Program for Frontier Research on Molecular, Destruction and Reconstruction of Tooth and Bone, Tokyo Medical and Dental University, 1-5-45 Yushima, Bunkyo-ku, Tokyo 113-8510; [4]Department of Basic Pathology, National Defense Medical College, 3-2, Namiki, Tokorozawa, Saitama 359-1192; [5]Bioinformatics Group, Genome Center, and [6]Department of Genetic Diagnosis, Cancer Institute, Japanese Foundation for Cancer Research, 3-10-6, Ariake Koto-ku, Tokyo 135-8550; [7]Department of Molecular Pharmacology, Medical Research Institute, Tokyo Medical and Dental University, 2-3-10, Kanda-Surugadai, Chiyoda-ku, Tokyo 101-0062

(Received December 12, 2006/Revised January 20, 2007/Accepted January 27, 2007/Online publication March 19, 2007)

An accurate assessment of the cervical lymph node metastasis status in oral cavity cancer not only helps predict the prognosis of patients, but also helps surgeons to perform the appropriate treatment. We investigated the utilization of microarray technology focusing on the differences in gene expression profiles between primary tumors of oral squamous cell carcinoma that had metastasized to cervical lymph nodes and those that had not metastasized in the hope of finding new biomarkers to serve for diagnosis and treatment of oral cavity cancer. To design this experiment, we prepared two groups: the learning case group with 30 patients and the test case group with 13 patients. All tissue samples were performed using laser captured microdissection to yield cancer cells, and RNA was isolated from purified cancer cells. To identify a predictive gene expression signature, the different gene expressions between the two groups with and without metastasis in the learning case ($n = 30$) were analyzed, and the 85 genes expressed differentially were selected. Subsequently, to construct a more accurate prediction model, we further selected the genes with a high power for prediction from the 85 genes using the AdaBoost algorithm. The eight candidate genes, *DCTD, IL-15, THBD, GSDML, SH3GL3, PTHLH, RP5-1022P6* and *C9orf46*, were selected to achieve the minimum error rate. Quantitative reverse transcription–polymerase chain reaction was carried out to validate the selected genes. From these statistical methods, the prediction model was constructed including the eight genes and this model was evaluated by using the test case group. The results in 12 of 13 cases (~92.3%) were predicted correctly. (*Cancer Sci* 2007; 98: 740–746)

In 2005, 335 870 Japanese people died from cancer. Of these, 5679 people had oral cavity cancer (http:www.mhlw.go.jp/toukei/saikin/hw/jinkou/suikei05/index.html) and the major cause of death by cancer was metastasis. An accurate assessment of the cervical lymph node metastasis status in oral cavity cancer not only helps predict the prognosis of patients, but also helps surgeons to carry out the appropriate treatment. When the disease is localized, surgical procedures can be used to remove the tumor in its entirety. For patients who are diagnosed clinically as cervical lymph node metastasis-positive (N+), a surgical procedure, known as radical neck dissection (RND), is used to remove all lymph node groups from levels I, II, III, IV and V, which involves the sacrifice of the internal jugular vein, sternocleidomastoid muscle and spinal accessory nerve.

The clinical diagnostic procedure for clinical staging of cervical lymph nodes is carried out by clinical examination of the neck region or by ultrasound, computed tomography and magnetic resonance imaging. But the sensitivity of these methods is still limited. Post-operative histological examination shows that approximately 30% of clinically diagnosed metastasis-negative (N0) patients have metastasis-positive lymph nodes in the neck,[1] and 10–20% of clinically diagnosed metastasis-positive (N+) patients turn out to be metastasis-free. Due to the fact that the false-negative rate is high in clinically diagnosed metastasis-negative (N0) patients, most surgeons would not like to select a 'wait and watch' policy, because it may allow metastasis to spread further. Thus, the surgeons usually carry out a supraomohyoid neck dissection (SOHND) to remove lymph nodes at levels I, II and III to screen for metastasis. Although SOHND is not as stringent as RND and the technique of neck dissection has been perfected over the last century, surgeons still face minor and major complications during the surgical procedure,[2] also sequelae such as chronic pain and limitation of shoulder movement due to a weak trapezius muscle.

Metastasis is a very complicated process. To metastasize, the cancer cells must break away from the tumor, increase their mobility and move through the extracellular matrix. Next they must invade the lymph vessels and grow in the lymph nodes or invade blood vessels and travel in the circulatory system. They then can pass through the vessel walls into surrounding tissue (distant metastasis). We think that the original genes controlling this process and the gene products of this process may be used as predictive markers of cervical lymph node metastasis. In the present study, microarray technology was used to investigate the differences in gene expression profiles between primary tumors of oral squamous cell carcinoma (OSCC) that metastasized to cervical lymph nodes and those that did not metastasize, in an effort to find new biomarkers that will provide more accurate diagnosis and more appropriate treatment for OSCC.

Materials and Methods

Tumor samples. All of the primary oral cancer specimens were obtained from anonymous patients who were previously untreated at the Faculty of Dentistry, Tokyo Medical and Dental University and were defined as squamous cell carcinoma of the oral cavity by histopathology. Informed consent was obtained from all of the patients. All clinical materials were approved by the ethics committee. The samples were embedded using Tissue-Tek OCT Compound (Sakura Finetek USA) and stored at −80°C until use. These samples were grouped into metastasis group and non-metastasis group based on clinical diagnosis and histological

*To whom correspondence should be addressed. E-mail: miki.mgen@mri.tmd.ac.jp

doi: 10.1111/j.1349-7006.2007.00454.x

Table 1. Clinical and histological characteristics of individual patients

Case	Sex	Age (years)	Primary site	TN	Differentiation	Prediction score
Learning case						
1	M	56	Lower gingival	T2N0	Moderately	−0.791
2	M	62	Buccal mucosa	T1N0	Well	−0.032
3	M	55	Upper gingival	T2N0	Well	−0.780
4	F	66	Tongue	T2N0	Moderately	−0.309
5	M	72	Hard palate	T1N0	Moderately	−0.481
6	M	58	Mouth floor	T2N0	Well	−0.716
7	M	80	Tongue	T2N0	Well	−0.564
8	M	30	Tongue	T2N0	Well	−0.609
9	F	81	retromolar trigone	T1N0	Well	−0.507
10	F	60	Tongue	T2N0	Well	−0.264
11	M	59	Tongue	T3N0	Moderately	−0.481
12	M	68	retromolar trigone	T2N0	Moderately	−0.428
13	M	54	Tongue	T1N0	Well	−0.534
14	M	56	Upper gingival	T2N0	Well	−0.303
15	M	43	Tongue	T2N0	Moderately	−0.716
16	M	46	Tongue	T2N0	Well	−0.564
17	M	58	Tongue	T2N0	Well	−0.282
18	F	64	Lower gingival	T4aN1	Well	0.348
19	M	66	Tongue	T1N2b	Moderately	0.411
20	M	77	Lower gingival	T2N2b	Poor	0.577
21	F	74	Buccal mucosa	T2N1	Moderately	0.780
22	M	78	Lower gingival	T2N1	Well	0.499
23	M	71	Buccal mucosa	T3N2b	Poor	0.499
24	M	71	Lower gingival	T3N2b	Well	0.564
25	M	61	Tongue	T2N2c	Moderately	0.318
26	M	60	Lower gingival	T4N2b	Moderately	1.000
27	M	57	Upper gingival	T4aN1	Poor	0.571
28	M	70	Tongue	T3N1	Moderately	0.592
29	M	52	Lower gingival	T4aN2b	Moderately	0.817
30	M	37	Tongue	T2N3	Poor	0.292
Test case						
1	M	66	Lower gingival	T2N0	Well	−0.318
2	F	66	Upper gingival	T2N0	Moderately	−0.288
3	M	73	Tongue	T2N0	Poor	−0.507
4	M	32	Tongue	T3N0	Moderately	−0.260
5	M	58	Mouth floor	T3N0	Moderately	−0.053
6	M	72	Lower gingival	T2N0	Well	−0.165
7	M	66	Mouth floor	T3N1	Moderately	0.162
8	M	68	Lower gingival	T4aN2b	Moderately	0.214
9	F	54	Tongue	T2N2b	Moderately	0.329
10	M	59	Mouth floor	T4N1	Moderately	0.115
11	M	67	Mouth floor	T4N1	Well	0.143
12	M	60	Tongue	T4N2c	Moderately	0.164
13	M	53	Tongue	T2N2b	Moderately	−0.228

T1, tumor ≤2 cm in greatest dimension; T2, tumor >2 cm but ≤4 cm in greatest dimension; T3, tumor >4 cm in greatest dimension; T4, (lip) tumor invades through cortical bone, inferior alveolar nerve, floor of mouth, or skin of face (i.e. chin or nose); T4a, (oral cavity) tumor invades adjacent structures (e.g. through cortical bone, into deep [extrinsic] muscle of tongue [genioglossus, hyoglossus, palatoglossus, and styloglossus], maxillary sinus, and skin of face); T4b, tumor invades masticator space, pterygoid plates, or skull base and/or encases internal carotid artery; N0, no regional lymph node metastasis; N1, metastasis in a single ipsilateral lymph node, ≤3 cm in greatest dimension; N2, metastasis in a single ipsilateral lymph node, >3 cm but ≤6 cm in greatest dimension, or in multiple ipsilateral lymph nodes, ≤6 cm in greatest dimension, or in bilateral or contralateral lymph nodes, ≤6 cm in greatest dimension; N2a, metastasis in a single ipsilateral lymph node >3 cm but ≤6 cm in dimension; N2b, metastasis in multiple ipsilateral lymph nodes, ≤6 m in greatest dimension; N2c, metastasis in bilateral or contralateral lymph nodes, ≤6 cm in greatest dimension; N3, metastasis in a lymph node >6 cm in greatest dimension.

examination. For the learning case, 30 samples were prepared (Table 1) including 13 samples from patients who were found to be N+ in the cervical lymph node and 17 samples from patients who were found to be N0 in the cervical lymph node. Those that remained metastasis-free were monitored for at least 1 year after the primary tumor was removed. (The primary tumors were surgically removed between April 2004 and October 2005.) For the test case, 13 samples were prepared (Table 1) including seven samples found to be N+ in the cervical lymph node and six samples found to be N0 in the cervical lymph node. Those remaining metastasis-free were monitored for at least 6 months after the primary tumor was removed. (The primary tumors were surgically removed between November 2005 and April 2006.) To determine the technical reproducibility, we prepared eight samples from the learning case for a replicate experiment.

Laser captured microdissection. All primary tumor specimens were cut into 9-μm sections at −20°C using a LEICA cryostat model 3050S. The sections were mounted on a special slide for use in laser captured microdissection (LCM) and immediately placed at −80°C before use. First, the sections were fixed in cold

ethanol for 3 min. They were then were washed in dionised water for 30 s, stained with hematoxylin for 40 s, and again washed in dionised water for 30 s. The sections were dried by cold wind for 2 or 3 min before the LCM. Squamous cell carcinomas were obtained accurately from the hematoxylin-stained tissue sections by LCM.

RNA isolation and quality assessment. Total RNA was extracted from the harvested cells using the RNeasy Micro Kit of Qiagen, and the concentration was measured using a NanoDrop ND-100 Spectrophotometer. All RNA was run with RNA 6000 Pico LabChip kits on the Agilent 2100 Bioanalyzer to analyze the quality of total RNA. The total RNA quality was assessed by RNA integrity number (RIN) value,[3,4] and the samples with RIN values below 5[5] were not used for the next step.

cRNA amplification and biotin labeling. Total RNA (100 ng) of each sample was used for starting the protocol of Two-Cycle cDNA Synthesis and labeling of cRNA, following the recommendations of Affymetrix.[6] The yield of biotin-labeled cRNA was measured using a NanoDrop ND-100 Spectrophotometer and the quality was analyzed using an Agilent 2100 Bioanalyzer. We removed samples with a yield less than 40 μg or with a median size of biotin-labeled cRNA fragments less than 500 bp.

Microarray production. The Human Genome U133 Plus 2.0 array was purchased from the Affymetrix company in Japan. The array comprised 1 300 000 distinct oligonucleotides and featured over 47 000 transcripts and variants, including approximately 39 000 of the best-characterized human genes.

Cocktail solution and microarray hybridization. Before making a cocktail solution, we used 20 μg of biotin-labeled cRNA and broke down the full length to 35–200 base fragments. Then, we used 15 μg of broken cRNA to make the cocktail solution, and the solution was put into GeneChip HG U133 plus 2 and hybridized for 16 h at 45°C. After hybridization, the arrays were washed and stained using Fluidic station 450 with protocol EukGE-WS2v5_450 and the arrays were scanned using the Affymetrix GeneChip Scaner 3000.

Statistical analysis. After scanning, the fluorescence intensity was measured using Affymetrix Microarray Suite 5.0 software, and the array was removed if it had a report with a scale factor larger than 6, 3′/5′ β-actin larger than 35 or 3′/5′ glyceraldehyde-3-phosphate dehydrogenase larger than 7. At low-level analysis, the arrays were imported into the RMAExpress software (http://rmaexpress.bmbolstad.com) to perform normalization using the RMA algorithm[7,8] and computing expression levels, because the RMA algorithm gave the most reproducible results and showed the highest correlation coefficients with real-time polymerase chain reaction data.[9,10] After the expression levels were calculated, the array data were imported into DNA-Chip analysis software (http://www.dchip.org) for high-level analysis. Gene filtering was carried out using the variation across samples criteria ($0.3 <$ standard deviation/mean < 100). For group comparison, two-group *t*-tests were used with a threshold of $P < 0.04$, absolute value of the difference in mean expression between two groups (Δ) > 100 intensity units and a fold change in mean expression >1.5 and <0.66. The 85 genes (Table 2) were selected. After selecting 85 genes that showed a difference in expression levels between the two groups, we again extracted from the 85 genes with software using the Adaboost algorithm.[11] The software was able to autoselect the best gene combination for separating the metastasis group from the non-metastasis group with the lowest cross validation (CV) error rate. Eight genes (Table 3) were extracted with a higher power for prediction, and were used to evaluate 13 samples from the test case.

Quantitative reverse transcription–polymerase chain reaction analysis. Quantitative reverse transcription–polymerase chain reaction (RT-PCR)[12] was to validate the results of eight meaningfully expressed genes from the analyzed microarray array data. For each sample, 100 ng of original total RNA was used to synthesize the first strand of cDNA by reverse transcriptase using oligo dT primer following the protocol recommended by Invitrogen (Superscript III First-Strand Synthesis System for RT-PCR). Primer sets for quantitative RT-PCR (Table 4) were designed

Table 2. The 85 genes related to lymph node metastasis

Accession no.	Gene symbol	Description	Fold change	*P*-value
Downregulated genes in the metastasis group				
NM_000597	*IGFBP2*	Insulin-like growth factor binding protein 2, 36 kDa	−6.81	0.004005
NM_002276	*KRT19*	Keratin 19	−5.78	0.028855
BG401568	*SLC16A9*	Solute carrier family 16 (monocarboxylic acid transporters), member 9	−3.54	0.000823
NM_001387	*DPYSL3*	Dihydropyrimidinase-like 3	−3.33	0.035334
NM_016140	*CGI-38*	Brain specific protein /// brain specific protein	−2.49	0.019781
NM_001823	*CKB*	Creatine kinase, brain	−2.42	0.006229
AF288571	*LEF1*	Lymphoid enhancer-binding factor 1	−2.35	0.033874
NM_002820	*PTHLH*	Parathyroid hormone-like hormone	−2.34	0.02038
AW451197		CDNA clone IMAGE:5278089	−2.32	0.035398
AI278995		Predicted: *Homo sapiens* similar to B230208J24Rik protein (LOC201501), mRNA	−2.24	0.01941
M31157	*PTHLH*	Parathyroid hormone-like hormone	−2.16	0.038689
NM_003027	*SH3GL3*	SH3-domain GRB2-like 3	−2.15	0.029178
AL567411	*CDK5R1*	Cyclin-dependent kinase 5, regulatory subunit 1 (p35)	−2.13	0.011045
BG434174		Stoned B-like factor	−2.11	0.023189
AI522132		Hypothetical protein LOC115749	−2.04	0.038373
BC005961	*PTHLH*	Parathyroid hormone-like hormone /// parathyroid hormone-like hormone	−2.00	0.022891
NM_001759	*CCND2*	Cyclin D2	−1.98	0.018311
BG290193	*ZNF703*	Zinc finger protein 703	−1.93	0.037675
AI189753	*TM4SF1*	Transmembrane 4 L six family member 1	−1.92	0.011249
AA143793	*RAB11FIP1*	RAB11 family interacting protein 1 (class I)	−1.89	0.013964
BF111651	*PPAPDC1B*	Phosphatidic acid phosphatase type 2 domain containing 1B	−1.89	0.03133
AL137763	*GRHL3*	Grainyhead-like 3 (Drosophila)	−1.89	0.035038
BC000408	*ACAT2*	Acetyl-Coenzyme A acetyltransferase 2 (acetoacetyl Coenzyme A thiolase)	−1.88	0.006495
AW026491	*CCND2*	Cyclin D2	−1.87	0.032209
AL137629	*KALRN*	Kalirin, RhoGEF kinase	−1.82	0.031132
BF514585	*SESN3*	Sestrin 3	−1.77	0.021875

doi: 10.1111/j.1349-7006.2007.00454.x

Table 2. *continued*

Accession no.	Gene symbol	Description	Fold change	*P*-value
M90657	*TM4SF1*	Transmembrane 4 L six family member 1	−1.76	0.011547
AI458128	*CBX6*	Chromobox homolog 6	−1.73	0.018388
BF680438	*LONRF1*	LON peptidase N-terminal domain and ring finger 1	−1.70	0.01133
AU154469	*SLC11A2*	Solute carrier family 11 (proton-coupled divalent metal ion transporters), member 2	−1.69	0.018722
BG165333	*CNKSR3*	CNKSR family member 3	−1.68	0.016795
AI654238	*B4GALNT3*	β1,4-*N*-acetylgalactosaminyltransferase-transferase-III	−1.63	0.018618
AI346835	*TM4SF1*	Transmembrane 4 L six family member 1	−1.52	0.006659
Upregulated genes in the metastasis group				
BE501952	*SATL1*	Spermidine/spermine N1-acetyl transferase-like 1	1.51	0.015987
AI809870	*SMYD2*	SET and MYND domain containing 2	1.54	0.003793
NM_017665	*ZCCHC10*	Zinc finger, CCHC domain containing 10	1.54	0.010698
BF214329		Mitochondrial fission regulator 1	1.56	0.008586
AI123233	*RANBP6*	RAN binding protein 6	1.58	0.0279
NM_016040	*TMED5*	Transmembrane emp24 protein transport domain containing 5	1.59	0.015651
NM_001889	*CRYZ*	Crystallin, zeta (quinone reductase)	1.59	0.012586
NM_013322	*SNX10*	Sorting nexin 10	1.59	0.028971
NM_024699	*ZFAND1*	Zinc finger, AN1-type domain 1	1.6	0.018314
U13700	*CASP1*	Caspase 1, apoptosis-related cysteine peptidase (interleukin 1, beta, convertase)	1.61	0.02315
AW157773	*ZFP62*	Zinc finger protein 62 homolog (mouse)	1.61	0.016554
NM_016283	*TAF9*	TAF9 RNA polymerase II, TATA box binding protein (TBP)-associated factor, 32 kDa	1.62	0.012154
BF439522	*MGC23909*	Hypothetical protein MGC23909	1.63	0.017789
NM_003187	*TAF9*	TAF9 RNA polymerase II, TATA box binding protein (TBP)-associated factor, 32 kDa	1.65	0.006175
NM_014873	*LPGAT1*	Lysophosphatidylglycerol acyltransferase 1	1.65	0.010458
AK001947	*RP5-1022P6.2*	Hypothetical protein KIAA1434	1.65	0.026428
NM_016576	*GMPR2*	Guanosine monophosphate reductase 2	1.66	0.039452
NM_024430	*PSTPIP2*	Proline-serine-threonine phosphatase interacting protein 2	1.67	0.016465
AW612657	*LYPLAL1*	Lysophospholipase-like 1	1.67	0.021165
L12723	*HSPA4*	Heat shock 70 kDa protein 4	1.69	0.006059
BC001025	*RCL1*	RNA terminal phosphate cyclase-like 1	1.71	0.007725
AI042152	*TncRNA*	Trophoblast-derived noncoding RNA	1.71	0.02217
AW962511	*FLJ22531*	Hypothetical protein FLJ22531	1.73	0.036123
AI634046	*CFLAR*	CASP8 and FADD-like apoptosis regulator	1.74	0.03599
AF183569	*ARTS-1*	Type 1 tumor necrosis factor receptor shedding aminopeptidase regulator	1.76	0.009405
AI805560	*ZMYM6*	Zinc finger, MYM-type 6	1.77	0.01367
AI347128	*IGBP1*	Immunoglobulin (CD79A) binding protein 1	1.77	0.001289
NM_002198	*IRF1*	Interferon regulatory factor 1	1.8	0.016707
NM_000361	*THBD*	Thrombomodulin	1.81	0.007352
NM_000361	*THBD*	Thrombomodulin	1.84	0.007352
NM_012485	*HMMR*	Hyaluronan-mediated motility receptor (RHAMM)	1.84	0.009623
BF735901	*NUDCD2*	NudC domain containing 2	1.86	0.00967
AL559202		Full-length cDNA clone CS0DF034YI03 of fetal brain of *Homo sapiens* (human)	1.86	0.009237
AW973232		gb:AW973232 /DB_XREF=gi:8163078 /DB_XREF=EST385330 /FEA=EST /CNT=5 /TID=Hs.293553.0 /TIER=ConsEnd /STK=0 /UG=Hs.293553 /UG_TITLE=ESTs	1.89	0.008534
NM_004120	*GBP2*	Guanylate binding protein 2, interferon-inducible /// guanylate binding protein 2, interferon-inducible	1.89	0.029524
U29343	*HMMR*	Hyaluronan-mediated motility receptor (RHAMM)	1.92	0.004741
AW119113	*THBD*	Thrombomodulin	1.92	0.010555
NM_018530	*GSDML*	Gasdermin-like	1.95	0.027119
NM_014349	*APOL3*	Apolipoprotein L, 3	1.95	0.018873
AI224133		Transcribed locus, weakly similar to XP_517454.1 PREDICTED: similar to hypothetical protein MGC45438 [Pan troglodytes]	1.96	0.039636
AI928035	*IRX2*	Iroquois homeobox protein 2	1.99	0.022852
NM_018465	*C9orf46*	Chromosome 9 open reading frame 46	1.99	0.014382
AW003140		mRNA; cDNA DKFZp686K1098 (from clone DKFZp686K1098)	2.04	0.025115
AW613387		Endothelial cell growth factor 1 (platelet-derived)	2.09	0.013803
NM_001657	*AREG*	Amphiregulin (schwannoma-derived growth factor)	2.10	0.013069
BC005254	*CLEC2B*	C-type lectin domain family 2, member B	2.11	0.024784
AI656493	*DCTD*	dCMP deaminase	2.17	0.004514
NM_005415	*SLC20A1*	Solute carrier family 20 (phosphate transporter), member 1	2.17	0.022575
NM_004815	*ARHGAP29*	Rho GTPase activating protein 29	2.27	0.009215
AA976354	*KIAA1618*	KIAA1618	2.61	0.017377
NM_000585	*IL15*	Interleukin 15	2.80	0.00711
AI539443	*STAT1*	Signal transducer and activator of transcription 1, 91 kDa	3.00	0.033578

Table 3. Genes selected for the prediction model

Accession	Gene symbol	Description	Fold change	*P*-value
AI656493	*DCTD*	dCMP deaminase	2.17	0.004514
NM_000585	*IL15*	Interleukin 15	2.80	0.00711
AW119113	*THBD*	Thrombomodulin	1.92	0.010555
NM_018530	*GSDML*	Gasdermin-like	1.92	0.027119
NM_003027	*SH3GL3*	SH3-domain GRB2-like 3	−2.15	0.029178
BC005961	*PTHLH*	Parathyroid hormone-like hormone	−2.00	0.022891
BE328402	*RP5-1022P6*	Hypothetical protein KIAA1434	1.92	0.020426
NM_018465	*C9orf46*	Chromosome 9 open reading frame 46	1.99	0.014382

Table 4. Primers for the genes used in real-time polymerase chain reaction

Gene symbol	Product size (bps)	Forward primer	Reverse primer
DCTD	113	ctgcgaggctcctgtttaat	aagcttttgactcggtctgc
IL15	103	acaaacatcactctgctgcttagac	ctgatccaaggtctgatcatcttct
THBD	105	agcacttgtgttgtctggtggt	tgtgcacacagagatagcatgaa
GSDML	149	tgaggcacgaattctctgtg	ggcagtgaggacagactggt
SH3GL3	103	gcttcctgtcctaaaagtcattggt	ctgaggaatataggccattcgttg
PTHLH	122	tgtggcttgtttatccttagctc	cttgccctaggttgtgaact
RP5-1022P6	104	caatgagctttgcacagtttga	tagtcccttagcttttgcctcttg
C9orf46	121	cttcctggtcccgattgttc	actcttttctgtttccagtatgtcctc
Actin	150	atgtggccgaggactttga	tgtgtggacttgggagagga

using PRIMER 3 software (http://www.genome.wi.mit.edu) and were synthesized by the Sigma Corporation. The PCR reaction was carried out using an ABI Prism 7900 Sequence Detection system with Power SYBR Green Master Mix (15 μL Power SYBR Green Master Mix, 0.3 μL with 5 μM of each primer, 5 μL cDNA, 9.4 μL water). For each sample, reactions were carried out in triplicate following the program: denaturation for 15 s at 95°C, and annealing and extension for 60 s at 60°C. Cumulative fluorescence was measured at the end of the extension phase of each cycle. Quantification was based on standard curves from serial dilution of human normal total RNA purchased from Stratagene Corporation. The results were normalized by to actin, and then compared with the microarray data of eight genes.

Results

To identify a predictive gene expression signature, 30 primary tumor samples (learning case group) located in the oral cavity region were analyzed. These included 13 samples from individuals who were found postoperatively to have metastasis in the lymph node of the neck, and 17 samples from individuals who were found postoperatively to have no metastasis in the lymph node of the neck and who remained metastasis-free when monitored for at least 1 year after primary tumor removal. The cancer cells of the tumor were obtained by LEM technology. Total RNA was isolated and its quality checked. We removed samples with RIN values below 5. At first, technical reproducibility was determined using eight samples from the training case. The technical replicates of the same two-sample comparison showed a high Pearson correlation coefficient. The lowest Pearson correlation coefficient was 0.9433 (Supplementary Fig. S1). This result indicated that the technical reproducibility of gene expression was high. To analyze the results of 30 primary tumors samples, two-group *t*-tests were used with a threshold of $P < 0.04$ and an absolute value of the difference in mean expression between the two groups (Δ) > 100 intensity units, with fold change in mean expression >1.5 and <0.66. The 85 genes expressed differentially between the two patient groups with and without cervical lymph node metastasis were selected (Table 2), including 33 genes that were downregulated and 52 genes that were upregulated in the metastasis group. Next, hierarchical clustering was carried out using 85 genes from the 30 samples by Pearson's correlation distance metric and average linkage (Fig. 1). Two major cluster branches were created. One major cluster included 16 non-metastasis samples and the other included 13 metastasis samples and one non-metastasis sample (missed clustering). Subsequently, to construct a more accurate and practical prediction model using a smaller number of genes, we selected further the genes with a high power for prediction from the 85 genes using AdaBoost algorithm.[11] In the AdaBoost algorithm, the optimal gene and its weight are determined in each boosting step, and the prediction model is constructed by weighted voting of the selected genes. We performed 1000 replicates of five-fold cross validation for the learning cases. Eight candidate genes (*DCTD*, *IL-15*, *THBD*, *GSDML*, *SH3GL3*, *PTHLH*, *RP5-1022P6* and *C9orf46*) were selected (Table 3), which achieved the minimum error rate. Next a prediction score was established for each sample (Table 1). Prediction scores have a value from −1 to 1, and the borderline is 0. A positive score indicates cervical lymph node metastasis, whereas a negative score indicates that the sample is metastasis-free. In the learning case, all 13 metastasis samples had positive scores and all 17 non-metastasis samples had negative scores (Fig. 2A). Microarray is an excellent tool that can analyze the expression of tens of thousands of genes. However it has some problems with accuracy and universal use. For the prediction system with high accuracy, verification that we could accurately analyze gene expression using this method was required. Thus, to confirm the prediction results, quantitative RT-PCR of the selected eight genes was carried out and normalized to actin before being compared by microarray data. The Pearson correlation values of the eight genes between microarray data and quantitative RT-PCR data were calculated and revealed to be over 0.73 (Table 5), showing a high correlation between microarray data and quantitative RT-PCR data in this study. We evaluated the prediction model by using the test case group. A prediction score was calculated for each sample using the prediction model constructed in this study (Fig. 2B). Six non-metastasis samples and six of the seven metastasis samples (~92.3%) were predicted correctly by the prediction model. Only one case (~7.7%) was a failure by this prediction model (circled in red in Fig. 2B).

doi: 10.1111/j.1349-7006.2007.00454.x

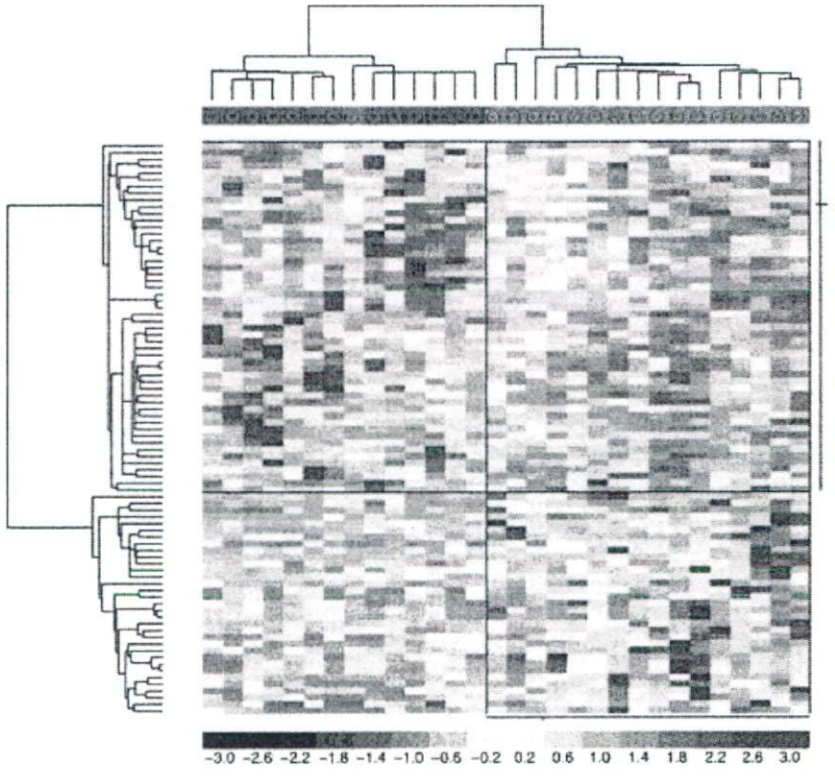

Fig. 1. Hierarchical clustering for 85 genes from 30 samples, including 13 metastasis samples (shown by pink color +) and 17 non-metastasis samples (shown by green color –). Red color shows that the gene is upregulated and blue color shows that the gene is downregulated. Two major cluster branches were created. One major cluster included 16 non-metastasis samples and the other one included 13 metastasis samples and one non-metastasis sample (missed clustering).

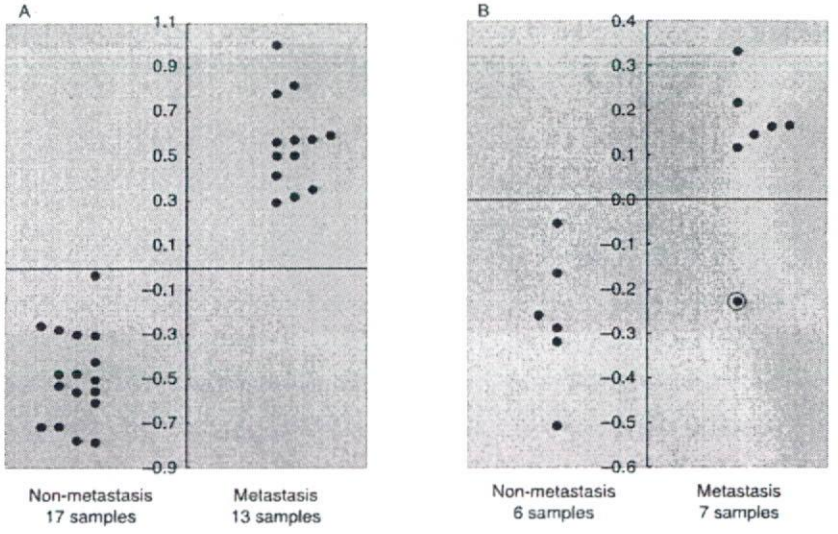

Fig. 2. The samples were rank-ordered by their score (determined by the Adaboost algorithm). A vertical line shows the total discriminant score. The samples with negative score indicated that the tumors were free of lymph node metastasis. The samples with positive scores indicated that the tumors metastasized to the cervical lymph node. (A) The prediction result of learning cases. All of the 17 samples in the non-metastasis group were negative and all of the 13 samples in the metastasis group were positive. (B) The prediction results of test cases. The six samples in the non-metastasis group were negative. Six of seven samples in the metastasis group were positive and one was negative (failure sample, circled in red).

Table 5. Pearson correlation of expression values between microarray data and real-time polymerase chain reaction data of the eight genes

Gene symbol	Pearson correlation	*P*-value
DCTD	0.796	2.46×10^{-7}
IL15	0.739	4.74×10^{-6}
THBD	0.753	2.49×10^{-6}
GSDML	0.868	1.06×10^{-9}
SH3GL3	0.911	6.86×10^{-12}
PTHLH	0.852	4.69×10^{-9}
RPS-1022P6	0.768	1.18×10^{-6}
C9orf46	0.742	4.05×10^{-6}

Discussion

At present, the methods for diagnosing the status of lymph node metastasis in oral cavity cancer are not accurate. Thus, two opinions were formed about the treatment of individual clinically diagnosed oral cavity cancer cases that are cervical lymph node metastasis-free. The first is the 'neck dissection' policy and the other is the 'wait and watch' policy. However, neither policy provides appropriate treatment for the disease. Because the neck dissection policy can cause pain, discomfort and in some cases leads to complications (such as chronic pain and shoulder palsy), it is important to ascertain whether a patient really is metastasis-free. The alternative 'wait and watch' policy may

allow an overlooked metastasis to spread widely for the patient who has micrometastasis. The goal of our study is to devise a novel diagnostic system that may improve the diagnosis of N status in oral cavity cancer. The results in 12 of 13 cases (~92.3%) were predicted correctly. Only one case (~7.7%) was a failure by this prediction model. The misjudged metastasis case using our prediction model was a 53-year-old man with moderately differentiated tongue squamous cell carcinoma. It is very difficult to discuss why the case missed, because we could not find any relationship between clinicopathological features of the patient and the score. In this study we would like to say that quantitative RT-PCR data should not be use for this prediction model system. The data could not be predicted accurately. The reason was that the prediction score from microarray data were normalized by RMA algorithm, but the quantitative RT-PCR data were normalized to actin; therefore the gene expression value of each gene by quantitative RT-PCR data differs from the microarray data.

Of the eight genes identified, *IL-15* is of particular interest. IL-15 is a cytokine that regulates T and natural killer cell activation and proliferation. Studies on mice suggest that IL-15 may increase the expression of apoptosis inhibitor. A recent study has reported that IL-15 expression has been shown to play an important role in cell proliferation, invasion and metastasis of human colorectal cancer.[13,14] In the present study, we observed IL-15 overexpression in the metastasis group (fold change [FC]: 2.8, $P < 0.00711$; Pearson correlation between microarray data and real-time PCR, 0.739). This showed that IL-15 may also play a role in the metastasis of oral squamous cell carcinoma. Further study is required to learn more about the roles of IL-15 in the metastasis of OSCC.

A second interesting gene is *PTHLH*. The protein encoded by this gene is a member of the parathyroid hormone family. This hormone regulates endochondral bone development and epithelial–mesenchymal interactions during formation of the mammary glands and teeth. Some articles have reported that PTHLH may play a role in metastasis of breast cancer and prostate cancer cell lines by upregulation.[15,16] But in our results, *PTHLH* was upregulated in the non-metastasis group and downregulated in the metastasis group (FC: −2, $P < 0.022891$; Pearson correlation between array data and real-time PCR, 0.852). It is difficult to explain why, but it may be that the *PTHLH* mechanism is different *in vitro* compared with *in vivo*, or it may be that the role of PTHLH in each type of cells is different. It could also be that cancer cells produce PTHLH to prompt cancer cell migration and invasion, but when the metastasis process is finished PTHLH is no longer necessary and so was downregulated in the metastasis group. Further study may clarify the role of *PTHLH* in OSCC.

The novel diagnosis system using gene sets may be applied in diagnosis of the disease. Further, the system may be also applied for other diseases in the future.

Acknowledgments

Many thanks to Drs Takashi Shimoji, Koichi Nagasaki, Kiyotsugu Yoshida, Masaru Uekusa and Fumiyuki Uematsu for helpful discussion during the preparation of this article. We also thank Professor Marie Cosgrove for having checked the English language of this paper.

References

1 Jones AS, Phillips DE, Helliwell TR, Roland NJ. Occult node metastases in head and neck squamous carcinoma. *Eur Arch Otorhinolaryngol* 1993; **250**: 446–9.
2 Genden EM, Ferlito A, Shaha AR *et al.* Complications of neck dissection. *Acta Otolaryngol* 2003; **123**: 795–801.
3 Mueller O, Lightfoot S, Schroeder A. RNA integrity number (RIN) standardization of RNA quality control. Agilent Application Note, May 1 2004. Publication no. 5989-1165EN. Available from URL: http://www.gene-quantification.de/RIN.pdf
4 Imbeaud S, Graudens E, Boulanger V *et al.* Towards standardization of RNA quality assessment using user-independent classifiers of microcapillary electrophoresis traces. *Nucleic Acids Res* 2005; **33**: e56.
5 Lee J, Hever A, Willhite D, Zlotnik A, Hevezi P. Effects of RNA degradation on gene expression analysis of human postmortem tissues. *FASEB J* 2005; **19**: 1356–8.
6 Technical note. GeneChip Eukaryotic Small Sample Target Labeling Assay Version II. Available from URL: http://genomics.msu.edu/RTSF/small_sample_labeling.pdf
7 Irizarry RA, Bolstad BM, Collin F, Cope LM, Hobbs B, Speed TP. Summaries of Affymetrix GeneChip probe level data. *Nucleic Acids Res* 2003; **31**: e15.
8 Li J, Spletter ML, Johnson JA. Dissecting tBHQ induced ARE-driven gene expression through long and short oligonucleotide arrays. *Physiol Genomics* 2005; **21**: 43–58.
9 Irizarry RA, Hobbs B, Collin F *et al.* Exploration, normalization, and summaries of high density oligonucleotide array probe level data. *Biostatistics* 2003; **4**: 249–64.
10 Millenaar FF, Okyere J, May ST, van Zanten M, Voesenek LA, Peeters AJ. How to decide? Different methods of calculating gene expression from short oligonucleotide array data will give different results. *BMC Bioinformatics* 2006; **7**: 137.
11 Freund Y, Schapire RE. A short introduction to boosting. *J. Japan. Soc. Artif. Intel.* 1999; **14**: 771–80.
12 Ginzinger DG. Gene quantification using real-time quantitative PCR: an emerging technology hits the mainstream. *Exp Hematol* 2002; **30**: 503–12.
13 Kuniyasu H, Ohmori H, Sasaki T *et al.* Production of interleukin 15 by human colon cancer cells is associated with induction of mucosal hyperplasia, angiogenesis, and metastasis. *Clin Cancer Res* 2003; **9**: 4802–10.
14 Kuniyasu H, Oue N, Nakae D *et al.* Interleukin-15 expression is associated with malignant potential in colon cancer cells. *Pathobiology* 2001; **69**: 86–95.
15 Shen X, Qian L, Falzon M. PTH-related protein enhances MCF-7 breast cancer cell adhesion, migration, and invasion via an intracrine pathway. *Exp Cell Res* 2004; **294**: 420–33.
16 Shen X, Falzon M. PTH-related protein modulates PC-3 prostate cancer cell adhesion and integrin subunit profile. *Mol Cell Endocrinol* 2003; **199**: 165–77.

Supplementary Material

The following supplementary material is available for this article:

Fig. S1. Replicated experiment of eight samples. The technical replicates of the same two-sample comparison, showed a high Pearson correlation coefficient.

This material is available as part of the online article from:

http://www.blackwell-synergy.com/doi/abs/10.1111/j.1349-7006.2007.00454.x

<http://www.blackwell-synergy.com/doi/abs/10.1111/j.1349-7006.2007.00454.x>

(This link will take you to the article abstract).

Please note: Blackwell Publishing are not responsible for the content or functionality of any supplementary materials supplied by the authors. Any queries (other than missing material) should be directed to the corresponding author for the article.

doi: 10.1111/j.1349-7006.2007.00454.x

One-step Nucleic Acid Amplification for Intraoperative Detection of Lymph Node Metastasis in Breast Cancer Patients

Masahiko Tsujimoto,[1] Kadzuki Nakabayashi,[14] Katsuhide Yoshidome,[2] Tomoyo Kaneko,[8] Takuji Iwase,[9] Futoshi Akiyama,[8] Yo Kato,[8] Hitoshi Tsuda,[12] Shigeto Ueda,[13] Kazuhiko Sato,[13] Yasuhiro Tamaki,[3] Shinzaburo Noguchi,[3] Tatsuki R. Kataoka,[4] Hiromu Nakajima,[5] Yoshifumi Komoike,[6] Hideo Inaji,[6] Koichiro Tsugawa,[11] Koyu Suzuki,[10] Seigo Nakamura,[11] Motonari Daitoh,[14] Yasuhiro Otomo,[14] and Nariaki Matsuura[7]

Abstract

Purpose: Detection of sentinel lymph node (SLN) metastasis in breast cancer patients has conventionally been determined by intraoperative histopathologic examination of frozen sections followed by definitive postoperative examination of permanent sections. The purpose of this study is to develop a more efficient method for intraoperative detection of lymph node metastasis.

Experimental Design: Cutoff values to distinguish macrometastasis, micrometastasis, and nonmetastasis were determined by measuring cytokeratin 19 (CK19) mRNA in histopathologically positive and negative lymph nodes using one-step nucleic acid amplification (OSNA). In an intraoperative clinical study involving six facilities, 325 lymph nodes (101 patients), including 81 SLNs, were divided into four blocks. Alternate blocks were used for the OSNA assay with CK19 mRNA, and the remaining blocks were used for H&E and CK19 immunohistochemistry–based three-level histopathologic examination. The results from the two methods were then compared.

Results: We established CK19 mRNA cutoff values of 2.5×10^2 and 5×10^3 copies/μL. In the clinical study, an overall concordance rate between the OSNA assay and the three-level histopathology was 98.2%. Similar results were obtained with 81 SLNs. The OSNA assay discriminated macrometastasis from micrometastasis. No false positive was observed in the OSNA assay of 144 histopathologically negative lymph nodes from pN0 patients, indicating an extremely low false positive for the OSNA assay.

Conclusion: The OSNA assay of half of a lymph node provided results similar to those of three-level histopathology. Clinical results indicate that the OSNA assay provides a useful intraoperative detection method of lymph node metastasis in breast cancer patients.

Authors' Affiliations: Departments of [1]Pathology and [2]Surgery, Osaka Police Hospital, [3]Department of Breast and Endocrine Surgery, Osaka University Graduate School of Medicine, Departments of [4]Pathology, [5]Clinical Laboratory, and [6]Surgery, Osaka Medical Center for Cancer and Cardiovascular Diseases, and [7]Department of Molecular Pathology, Osaka University Graduate School of Medicine and Health Science, Osaka, Japan; Departments of [8]Pathology and [9]Breast Surgery, Cancer Institute of the Japanese Foundation for Cancer Research, and Departments of [10]Pathology and [11]Breast Surgical Oncology, St. Luke's International Hospital, Tokyo, Japan; Departments of [12]Pathology II and [13]Surgery I, National Defense Medical College, Saitama, Japan; and [14]Central Research Laboratories, Sysmex Corp., Kobe, Japan

Received 10/16/06; revised 4/3/07; accepted 5/15/07.

The costs of publication of this article were defrayed in part by the payment of page charges. This article must therefore be hereby marked *advertisement* in accordance with 18 U.S.C. Section 1734 solely to indicate this fact.

Note: Supplementary data for this article are available at Clinical Cancer Research Online (http://clincancerres.aacrjournals.org/).

M. Tsujimoto and K. Nakabayashi contributed equally to this work.

Requests for reprints: Nariaki Matsuura, Department of Molecular Pathology, Graduate School of Medicine and Health Science, Osaka University, 1-7 Yamadaoka, Suita, Osaka 565-0817, Japan. E-mail: matsuura@sahs.med.osaka-u.ac.jp.

doi:10.1158/1078-0432.CCR-06-2512

Sentinel lymph node (SLN) biopsy has recently become a standard surgical procedure in the treatment of breast cancer patients (1–10). This procedure can predict metastasis to the regional lymph nodes with high accuracy and avoids unnecessary removal of axillary lymph nodes and subsequent morbidity associated with axially clearance in node negative breast cancer patients.

SLN metastasis is generally detected by conventional means including the intraoperative H&E-based histopathologic examination of frozen section(s) or cytologic observation of touch-imprints, followed by definitive postoperative histopathologic examination of permanent sections (2, 7–9). However, the sensitivity of these intraoperative methods is not high. Many investigators have reported that the intraoperative H&E-based histopathologic examination has a false-negative rate of 5% to 52% (reviewed in ref. 11). Furthermore, these methods provide subjective rather than objective results, which may differ from one pathologist to another (12). On the other hand, the definitive postoperative histopathologic examination generally requires 5 to 10 days for assessment. If an accurate

intraoperative method is developed, the test results can allow for completion of axillary node dissection during surgery and avoidance of a second surgical procedure in patients with positive SLNs, thereby reducing patient distress and, finally, saving hospital costs (2, 13, 14). Accordingly, the development of a precise and objective intraoperative method for the detection of lymph node metastasis is important for increasing the efficiency of breast cancer surgery (10, 13–18).

To overcome the shortcomings of the present histopathologic methods, molecular biological methods based on quantitative reverse transcription-PCR (QRT-PCR) have been studied extensively for the detection of lymph node metastasis in breast cancer patients (12, 19–25). A QRT-PCR assay with multiple mRNA markers including cytokeratin 19 (CK19), trefoil factor 3 (p1B), epithelial glycoprotein 2 (EGP2), and small breast epithelial mucin (SBEM) resulted in a 10% upstaging compared with the routine histopathologic analysis (22). It was also reported that a QRT-PCR assay using mRNA markers of CK19 and mammaglobin 1 (MGB1) was almost as accurate (94.1% sensitivity and 98.6% specificity) as that of the conventional histopathologic examination (12). This study included a discussion of the drawbacks of using a single marker like CK19 mRNA for which the QRT-PCR may include the concomitant amplification of CK19 pseudogenes within genomic DNA, giving false positive results.

We recently developed a one-step nucleic acid amplification (OSNA) assay (Fig. 1A), which consists of solubilization of a lymph node followed by reverse-transcription loop-mediated isothermal amplification (RT-LAMP) of a target mRNA (26, 27). The RT-LAMP reaction is a new method of gene amplification, and its application has been reported previously (28–32). The OSNA method is characterized by the quantitative measurement of a target mRNA in a metastatic lymph node, a brief reaction time for the OSNA process, a high specificity for the target mRNA, and an absence of genomic DNA amplification.

In this paper, we report an efficient intraoperative detection method for lymph node metastasis in breast cancer patients using the OSNA assay with CK19 mRNA as a target marker. The results of a multicenter clinical study including 325 lymph nodes are discussed from the viewpoint of the usefulness of the OSNA assay as an intraoperative detection method.

Materials and Methods

Lymph nodes for selection of mRNA markers and determination of cutoff values. Lymph nodes, which were used to select mRNA markers and determine cutoff values, were obtained from Osaka Police Hospital with the approval of its internal review board. Lymph nodes were stored at -80°C until use.

QRT-PCR. QRT-PCR was carried out by ABI Prism 7700 sequence detector. RNA was purified from a lymph node lysate using RNeasy Mini Kit (Qiagen), and then purified RNA was subjected to one-step RT-PCR with QuantiTect SYBR Green (Qiagen) according to the manufacturer's instructions. The sequences of the forward and reverse primers used are shown in Supplementary Table S1. The primers were designed by Primer Express Version 2.0 software (ABI).

Selection of mRNA maker. Forty-five candidate mRNA markers, selected as being specific to breast cancer tissue, were identified from the public EST database (33). The performance of these mRNA markers was evaluated with QRT-PCR using a mixture of four histopathologically positive and four negative lymph nodes. The results were summarized as C_t (threshold cycle) values for each mRNA marker (see Supplementary Table S2). The selected markers, KRT19 (CK19), CEACAM5 (CEA), forkhead box A1 (FOXA1), SAM-pointed domain containing ETS transcription factor (SPDEF), tumor-associated calcium signal transducer 2 (TACSTD-2), mucin 1 (MUC1), and MGB1, were further evaluated with QRT-PCR using 11 histopathologically positive and 15 negative lymph nodes from 26 patients.

RT-LAMP reaction of CK19 mRNA. The RT-LAMP reaction was carried out according to the Notomi's method (26, 27). The human CK19 mRNA was synthesized by *in vitro* transcription from cloned cDNA.

A 2-μL sample of human CK19 mRNA in a lysis buffer containing 200 mmol/L glycine-HCl, 20% DMSO, and 5% Brij35 (pH 3.5) was added to 23 μL of solution consisting of 3.5 μmol/L each of the forward inner (CK19FA) and reverse primer (CK19RA), 0.2 μmol/L each of forward outer (CK19F3) and reverse primer (CK19R3), 2.6 μmol/L each of forward loop (CK19LPF) and reverse primer (CK19LPR), 0.9 mmol/L deoxynucleotide triphosphates, 54.3 mmol/L Tris-HCl, 10.8 mmol/L KCl, 10.8 mmol/L $(NH_4)_2SO_4$, 5.4 mmol/L $MgSO_4$, 0.1% Triton X-100, 5.4 mmol/L DTT, 2.5 units avian myeloblastosis virus reverse transcriptase (Promega), 18 units Bst DNA Polymerase (New England Biolabs), and 25 units RNasin Plus (Promega). Each reaction mixture contained three pairs of primer sets including the loop primer (27). The sequences of the human CK19 primers were designed as amplicons spanning exon junction regions between CK19 exons 1 and 2 and were

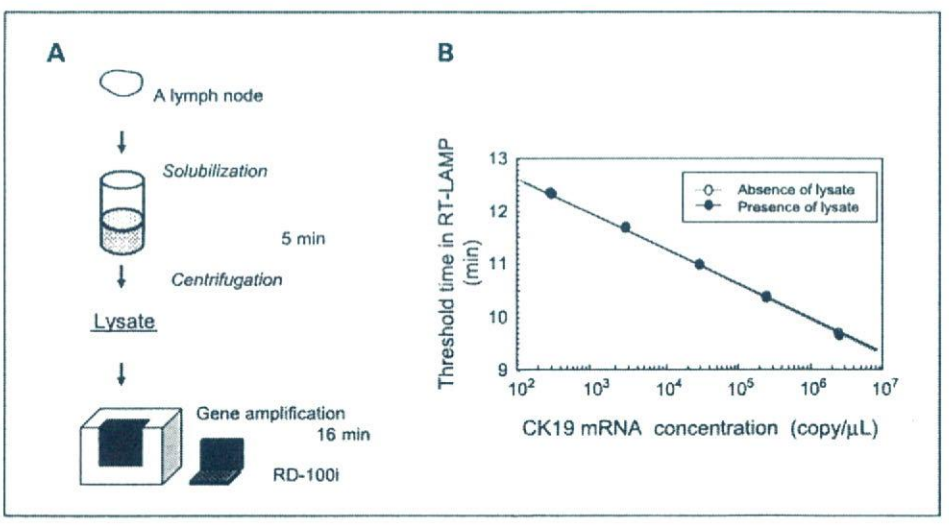

Fig. 1. OSNA assay. *A*, schematic diagram of the OSNA procedure. *B*, standard curve of human CK19 mRNA measured by RD-100i in the presence and absence of lymph node lysate. A histopathologically negative lymph node (600 mg) was homogenized in 4 mL of lysis buffer. A 180-μL sample of the lymph node lysate was added to 20 μL of human CK19 mRNA in the lysis buffer. The final concentration of human CK19 mRNA was adjusted to 2.5×10^6, 2.5×10^5, 2.5×10^4, 2.5×10^3, and 2.5×10^2 copies/μL. A 2-μL sample of each was subjected to the RT-LAMP reaction under the same conditions described in Materials and Methods.

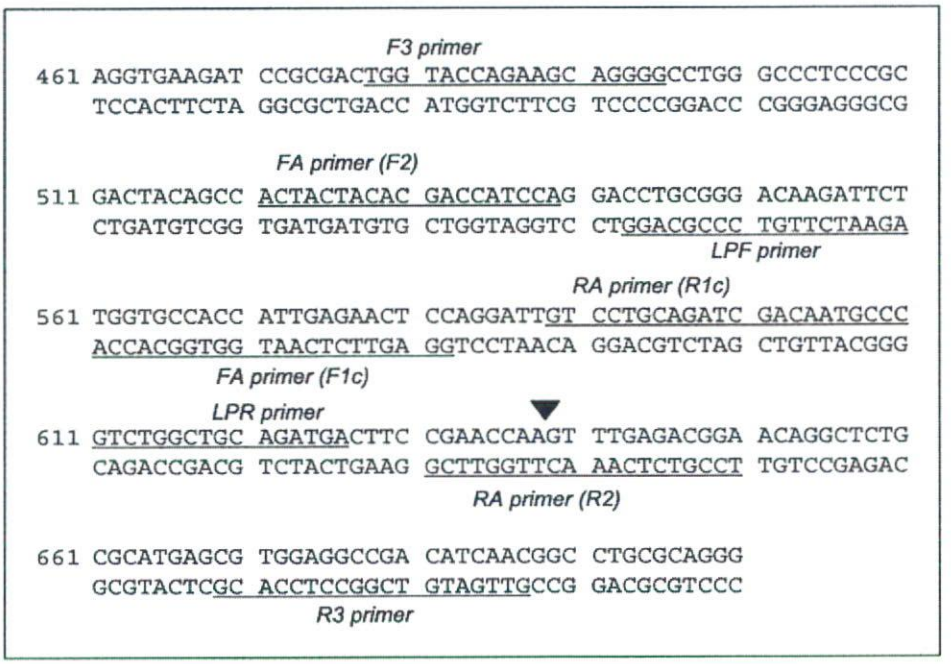

Fig. 2. A schematic representation of primer placement along the CK19 cDNA sequence. The CK19 cDNA sequence (NM.002276) and the sequence of the primers for the CK19 RT-LAMP are shown. The location on CK19 cDNA where each primer-set binds is underlined. The sequence of the inner primer (FA and RA) consists of discontinuous two different regions, F1c and F2 (or R1c and R2), to create the stem structure during the RT-LAMP reaction. The exon junction between exons 2 and 3 is included in the sequence of the R2 region in the RA primer (*arrowhead*).

furthermore designed as mismatch sequences of the CK19a and CK19b pseudogenes (GenBank accession number M33101 and U85961) using Probe Wizard (RNAture). Primer sequences were 5′-GGAGTTCT-CAATGGTGGCACCAACTACTACACGACCATCCA-3′ (CK19FA), 5′-GTCCTGCAGATCGACAACGCCTCCGTCTCAAACTTGGTTCG-3′ (CK19RA), 5′-TGGTACCAGAAGCAGGGG-3′ (CK19F3), 5′-GTTGATGTCGGCCTCCACG-3′ (CK19R3), 5′-AGAATCTTGTCCCG-CAGG-3′ (CK19LPF), and 5′-CGTCTGGCTGCAGATGA-3′ (CK19LPR). The sequence of each primer and its placement along the CK19 cDNA sequence are shown in Fig. 2.

The RT-LAMP reaction with CK19 mRNA was carried out in a gene amplification detector, RD-100i (Sysmex). Mori et al. (34, 35) reported that PPi, which is produced in the course of the RT-LAMP reaction, binds to magnesium ion to result in magnesium PPi. The amount of magnesium PPi increases with the passage of the reaction. Magnesium PPi has a low solubility in aqueous solution and precipitates when its concentration reaches saturation. The amplification of CK19 mRNA was monitored by measuring the turbidity of the reaction mixture at 6-s intervals. The threshold time was defined as the time at which the turbidity exceeded 0.1.

OSNA assay. A schematic diagram of the OSNA assay with CK19 mRNA is shown in Fig. 1A. A histopathologically negative lymph node (≤600 mg) was homogenized in 4 mL of the above lysis buffer for 90 s on ice using a Physicotron Warring blender with an NS-4 shaft (MicroTec Nichion). The homogenate was centrifuged at 10,000 × *g* for 1 min at room temperature. A 2-μL sample of the supernatant (lysate) was subjected to the RT-LAMP reaction under the same conditions as above. CK19 mRNA copy number was determined based on the standard curve using a known quantity of human CK19 mRNA.

Effect of lymph node size on the OSNA assay. A histopathologically negative lymph node (130 mg) was homogenized in 4 mL of lysis buffer under the same conditions as above. A 180-μL sample of lymph node lysate was added to 20 μL of human CK19 mRNA in the lysis buffer. The final concentration of human CK19 mRNA was adjusted to 2.5×10^5 and 2.5×10^3 copies/μL. About 2 μL of each sample was subjected to the RT-LAMP reaction under the same conditions described above. Each sample was assayed in duplicate. Other histopathologically negative lymph nodes (214, 354, and 428 mg) were treated under the same conditions as above.

Amplification of genomic DNA by the OSNA assay. Genomic DNA was extracted from histopathologically positive lymph nodes using QIAamp DNA Mini Kit (Qiagen) according to the manufacturer's instructions. Purified genomic DNA (100 ng) was subjected to the OSNA assay using the CK19 primers described above.

Protocol for determining the cutoff values. A cutoff value (*L*) for the OSNA assay between metastatic positive and negative lymph nodes was determined using 106 lymph nodes (42 histopathologically negative lymph nodes from pN0 patients, 42 histopathologically negative lymph nodes from pN1-3 patients, and 22 histopathologically positive lymph nodes) from 30 patients (24 ductal carcinomas, 5 special types, and 1 ductal carcinoma *in situ*). As shown in Fig. 3A, the central part of one quarter of a frozen lymph node (40-600 mg) of 1 mm thickness was dissected out. Four levels (i, ii, iii, and iv) were used as permanent slices for the histopathologic examination with H&E and immunohistochemistry using anti-CK19 antibody (DAKO) as shown in Fig. 3A.

Histopathologically positive lymph nodes were defined as those that were positive at any of four levels (i, ii, iii, and iv). Histopathologically negative lymph nodes were defined as those that were negative in all four levels. Blocks a and c were used for the OSNA assay. A cutoff value was determined by statistical analysis of the copy numbers obtained by the OSNA assay of the histopathologically negative lymph nodes from pN0 patients.

According to the tumor-node-metastasis (TNM) classification of the Unio Internationale Contra Cancrum (Italian) sixth and the American Joint Committee on Cancer sixth editions (36), macrometastasis is defined as having metastatic foci of ≥2 mm in the long axis. In the OSNA assay, macrometastasis is assumed as having the amount of CK19 mRNA expression in 2^3 mm^3 of metastatic foci. Based on this assumption, we estimated a cutoff value (*H*) for CK19 mRNA between macrometastasis and micrometastasis as follows. Nine frozen histopathologically positive lymph nodes from nine breast cancer patients (8 ductal and 1 lobular carcinomas) were used to estimate the amount of CK19 mRNA expression in 2^3 mm^3 of metastatic foci (Table 1). A frozen lymph node was serially sectioned at 10-μm intervals. Each slice was first examined with CK19 immunohistochemistry–based histopathologic examination to measure the area of metastatic foci and then with RT-LAMP to measure CK19 mRNA expression. The procedure is detailed in Fig. 3B.

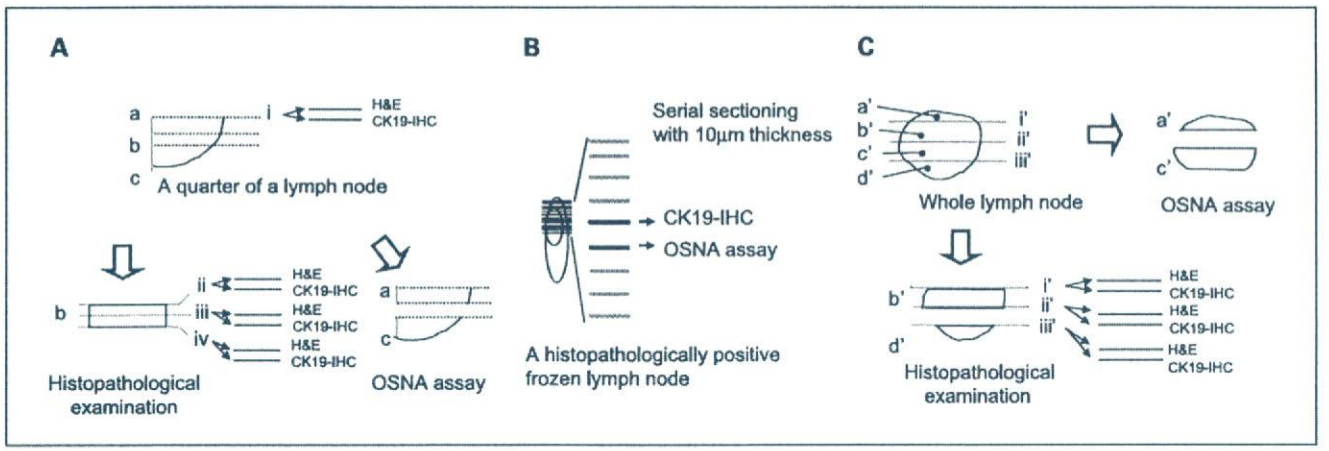

Fig. 3. Protocols. *A*, protocol for determining a cutoff value for micrometastasis and nonmetastasis. *B*, protocol for determining the cutoff value between macrometastasis and micrometastasis. Serial frozen sections taken at 10-μm intervals were prepared from histopathologically positive lymph nodes. One of two consecutive frozen sections was subjected to CK19 immunohistochemistry (CK19-IHC) – based histopathologic examination to measure the area of metastatic foci, and then the volume of the metastatic foci was calculated by multiplying the area by the thickness of the slice. The adjacent section was subjected to the OSNA assay. The expression level of CK19 mRNA in 2^3 mm^3 was estimated based on the correlation between the volume of metastatic foci and CK19 mRNA expression. *C*, clinical study protocol.

In the OSNA assay, an amount of CK19 mRNA expression less than the cutoff value was indicated as (-), an amount of CK19 mRNA expression between the cutoff values *L* and *H* was indicated as (+), and an amount of CK19 mRNA expression greater than the cutoff value *H* was indicated as (++).

Clinical study protocol. An intraoperative clinical study was conducted from February 2005 to July 2005 at six facilities other than Sysmex Central Research Laboratories. A total of 325 fresh lymph nodes (101 patients), including 81 SLNs (49 patients), were used with the approval of the internal review board at each facility. The clinicopathologic characteristics of patients are shown in Table 2. A large percent of patients had stages I A/B and II A/B. The majority of patients had a nodal status of pN0 and pN1. About 80% of patients had invasive ductal carcinoma.

A fresh lymph node with a short axis of 4 to 12 mm was divided into four blocks at 1- or 2-mm intervals using our original cutting device (Fig. 3C and 4). Blocks a′ and c′ were used for the OSNA assay. Two slices were cut from each of the three cutting surfaces (i′, ii′, and iii′), as shown in Fig. 3C, and used for the permanent three-level histopathologic examination with H&E and CK19 immunohistochemistry.

In the histopathologic examination, macrometastasis and micrometastasis were defined according to the TNM classification of the Unio Internationale Contra Cancrum sixth and American Joint Committee on Cancer sixth editions (36). All samples for histopathologic examination were examined by three third-party pathologists. Conflicting results were settled consensually. The performance of the OSNA assay was compared with the three-level histopathology.

The OSNA assay analyzed different blocks from those used in the three-level histopathologic examination. Therefore, in this protocol, the sensitivity and specificity of the OSNA assay could not be calculated based on the histopathologic results. For this reason, we evaluated the performance of the OSNA assay as a concordance rate with the three-level histopathologic examination.

In the case of lymph nodes from pN0 patients, blocks b′ and d′ were further sliced at 0.2-mm intervals, followed by staining each alternate slice with H&E and CK19 immunohistochemistry (Fig. 3C). A total of 144 lymph nodes, in which neither macrometastasis nor micrometastasis were observed in the above serial sectioning examination, were used for the false positive study of the OSNA assay.

When discordance between the OSNA assay and the three-level histopathologic examination occurred, a histopathologic analysis of blocks b′ and d′ was repeated. All slides for the histopathologic examination were examined and evaluated by three third-party pathologists. All results of histopathologic examinations were finally determined by a study group comprised of representatives from the different facilities.

Analysis of discordant cases. In the analysis of discordant cases, QRT-PCR and CK19 Western blot analysis of the lysates were carried out. QRT-PCR was carried out with TaqMan RT-PCR. RNA was purified from lymph node lysates using RNeasy Mini Kit (Qiagen), and then the purified RNA was subjected to TaqMan one-step RT-PCR universal master mix (ABI) according to the manufacturer's instructions. The sequences of the forward and reverse primers designed for human CK19 were 5′-CAGATCGAAGGCCTGAAGGA-3′ and 5′-CTTGGCCCCT-CAGCGTACT-3′, respectively. The sequence of the TaqMan probe, containing a fluorescent reporter dye (FAM) at the 5′ end and a fluorescent quencher dye (TAMRA) at the 3′ end, was 5′-FAM-GCCTACCTGAA-GAAGAACCATGAGGAGGAA-TAMRA-3′. The primers and TaqMan probe were obtained from Applied Biosystems (ABI). All QRT-PCR reactions were done in duplicate.

In the CK19 Western blot analysis, lysate (20 μL) was added to 10 μL of loading buffer containing 150 mmol/L Tris-HCl, 300 mmol/L DTT, 6% SDS, 0.3% bromophenol blue, and 30% glycerol. The solution was boiled and electrophoresed on a polyacrylamide gel in the presence of

Table 1. CK19 mRNA expression in 2^3 mm^3 of metastatic foci

Case	Histology	CK19 mRNA (copy/μL)
1	Ductal carcinoma	2.3×10^4
2	Ductal carcinoma	1.1×10^4
3	Ductal carcinoma	4.7×10^3
4	Ductal carcinoma	5.0×10^4
5	Ductal carcinoma	1.0×10^4
6	Lobular carcinoma	1.4×10^5
7	Ductal carcinoma	2.0×10^4
8	Ductal carcinoma	6.7×10^4
9	Ductal carcinoma	2.4×10^4
	Average	3.0×10^4

NOTE: CK19 mRNA expression in 2^3 mm^3 of metastatic foci was estimated on the basis of the examination of serial sections (Fig. 3B).

Table 2. Clinicopathologic characteristics of patients

	Number of patients
Stage	
0	5
I A/B	41
II A/B	49
III A/B/C	5
IV	1
Nodal status	
pN0	60
pN1	35
pN2	2
pN3	4
Histopathologic type	
Invasive ductal carcinoma	87
Neuroendocrine carcinoma	1
Matrix producing carcinoma	1
Mucinous carcinoma	2
Apocrine carcinoma	1
Invasive lobular carcinoma	4
Ductal carcinoma *in situ*	5

SDS (PAG Mini; Daiichi Pure Chemicals). After electrotransfer to Immobilon-FL polyvinylidene difluoride membranes (Millipore), the membrane was blocked with skim milk (BD Bioscience) for 1 h at room temperature. The primary antibody, anti-CK19 (A53-B/A2; Santa Cruz Biotechnology), was diluted 1:500 with TBS-Tween 20 (TBS-T) solution, and the membrane was incubated at 4°C overnight with anti-CK19 antibody. The membrane was then washed with TBS-T and incubated with a secondary antibody conjugated with horseradish peroxidase, which was diluted 1:2,000 with TBS-T. After washing the membrane twice with TBS-T, CK19-CK19 antibody complex was visualized using the ECL-Advance detection kit (GE Healthcare). The intensity of the signal in each band was evaluated by LumiAnalyst (Roche). CK19 protein concentration was determined based on a standard curve that was obtained by measuring known quantities of CK19 protein (Biodesign) of 0.15, 0.075, 0.038, and 0.018 ng/μL.

A cutoff value for CK19 protein expression between histopathologically positive and negative lymph nodes was determined by Western blot analysis of 37 histopathologically negative lymph nodes from 16 pN0 patients, 54 histopathologically negative lymph nodes from 17 pN1-3 patients, and 22 histopathologically positive lymph nodes from 12 patients (Figs. 3A and 5A). The cutoff value was determined by statistical analysis of the amount of CK19 measured by Western blot analysis of 37 histopathologically negative lymph nodes from 16 pN0 patients.

Results

Selection of the mRNA marker. We evaluated mRNAs for CK19, CEA, FOXA1, SPDEF, MUC1, and MGB1 using 11 histopathologically positive and 15 negative lymph nodes from 26 patients. The absolute mRNA expression levels of CEA and MGB1 in metastatic lymph nodes were not as high as expected, whereas the absolute expression levels of MUC1 mRNA in nonmetastatic lymph nodes was relatively high. For these reasons, CEA, MGB1, and MUC1 mRNAs were not selected for the OSNA assay.

The expression levels of CK19, FOXA1, and SPDEF mRNAs differed between histopathologically positive and negative lymph nodes. However, the lower limits of the expression levels of FOXA1 and SPDEF mRNAs in histopathologically positive lymph nodes were 4 to 30 times less than that of CK19 mRNA (Fig. 6). On the other hand, the detection limit of the OSNA assay was nearly equivalent to 32 threshold cycles of the RT-PCR system. An assay system should detect the upper limit of the expression levels of an mRNA marker in histopathologically negative lymph nodes. The upper limits of the threshold cycle of FOXA1 and SPDEF mRNAs were about 35 and 32,

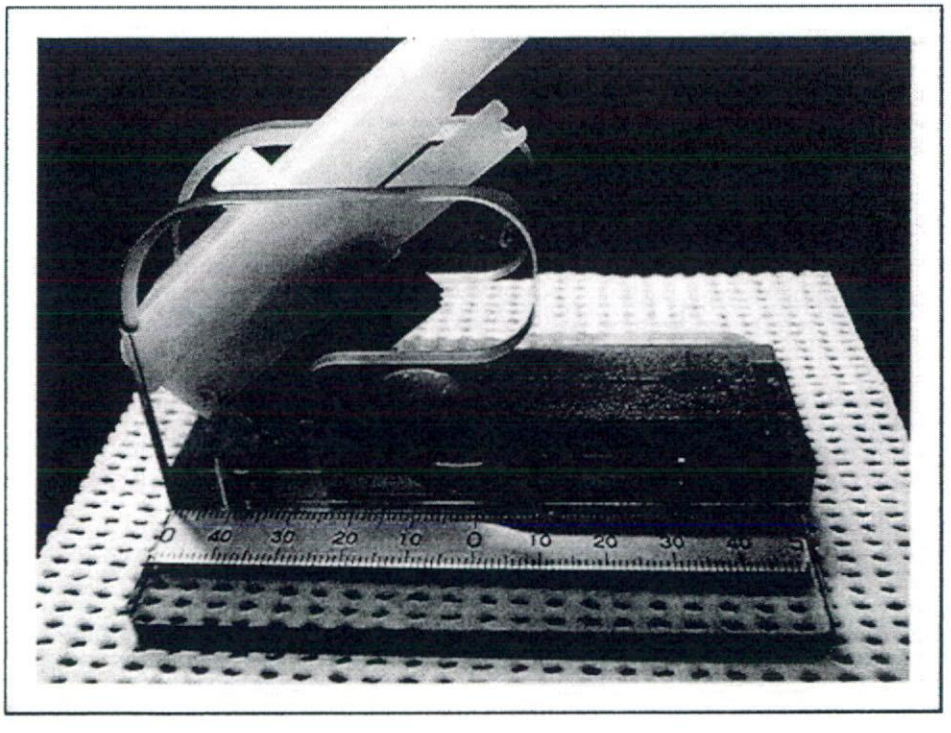

Fig. 4. Lymph node cutting device.

respectively. For these reasons, we determined CK19 mRNA to be the best marker for the OSNA assay.

OSNA assay. As shown in Fig. 1B, an inverse correlation between the threshold time in the RT-LAMP step and CK19 mRNA concentration was observed in a range of CK19 mRNA concentrations of 2.5×10^2 to 2.5×10^6 copies/μL, and both curves overlapped completely in the presence and absence of the lymph node lysate; the correlation coefficient value in both cases was 0.99. This result indicates that factors that may be present in lymph node lysates do not interfere with the OSNA assay.

Effect of lymph node size on the OSNA assay. The threshold time of the OSNA assay with 2.5×10^3 and 2.5×10^5 copies/μL of CK19 mRNA in a lysate obtained from 130 mg of lymph node was 10.9 and 9.6 min, respectively. The threshold time with 2.5×10^3 copies/μL of CK19 mRNA in a lysate obtained from a lymph node of 214, 354, and 428 mg was 10.7, 10.9, and 10.9 min, respectively, whereas the time with 2.5×10^5 copies/μL of CK19 mRNA in a lysate obtained from a lymph node of 214, 354, and 428 mg was 9.6, 9.7, and 9.7 min, respectively. The threshold times with 2.5×10^3 and 2.5×10^5 copies/μL of human CK19 mRNA in the lysates obtained from lymph nodes of 130, 214, 354, and 428 mg were within an acceptable error range. The results indicate that the OSNA assay is not influenced by lymph node size.

Amplification of genomic DNA by the OSNA assay. To exclude the possibility of genomic DNA amplification in the OSNA assay, we examined the OSNA assay using genomic DNA purified from lymph nodes. Genomic DNA was not amplified from either metastatic or nonmetastatic lymph nodes. The results indicate that the OSNA assay amplifies only CK19 mRNA.

Cutoff values. A cutoff value for the OSNA assay between histopathologically positive and negative lymph nodes was determined by the logarithmic normal distribution of CK19 mRNA copy numbers from 42 lymph nodes from pN0 patients. The average value of CK19 mRNA expression +3 SD was 2.5×10^2 copies/μL. Based on this analysis, we set the cutoff value at 2.5×10^2 copies/μL, which represents the upper limit of the copy numbers in the histopathologically negative lymph nodes from pN0 patients (Fig. 7A).

To validate the cutoff value, we examined CK19 mRNA expression in 42 histopathologically negative lymph nodes from 16 pN1-3 patients. Only one of these 42 cases showed $>2.5 \times 10^2$ copies/μL CK19 mRNA (Fig. 7B). This lymph node showed 3×10^3 copies/μL of CK19 mRNA. This suggested that micrometastatic foci in block a or c (Fig. 3A) of the lymph node were included in the sample. On the other hand, CK19 mRNA expression in all 24 pathologically positive lymph nodes from 10 patients exceeded the cutoff value (Fig. 7C).

To obtain a cutoff value for CK19 mRNA expression between macrometastasis with metastatic foci $>2^3$ mm^3 and micrometastasis, we compared CK19 mRNA expression in serial sections of a lymph node with an area of metastatic foci and roughly estimated macrometastasis to be $>5 \times 10^3$ copies/μL, which is the lowest value of CK19 mRNA expression found in metastatic foci of 2^3 mm^3 (Table 1).

Accordingly, for the OSNA assay, we defined macrometastasis (++) as $>5 \times 10^3$ copies/μL of CK19 mRNA, micrometastasis (+) as 2.5×10^2 to 5×10^3 copies/μL, and nonmetastasis (-) as $<2.5 \times 10^2$ copies/μL.

Clinical study. All OSNA assays were carried out during surgery and were completed within 30 min. H&E and CK19 immunohistochemistry were used in the histopathologic examination.

Isolated tumor cells (ITC) are widely used as one of indicators in a nomogram-aiding treatment decisions. In the American Society of Clinical Oncology guidelines (10), ITCs are described as having unknown clinical significance, and there are insufficient data to recommend appropriate treatment, including axillary lymph node dissection. For this reason, we viewed ITC as negative.

Table 3 shows the results of CK19 immunohistochemistry in all samples with the H&E results given in parenthesis. H&E-based histopathology failed to detect 1 of 40 cases of macrometastasis and 3 of 5 cases of micrometastasis. Overall, the sensitivity of H&E-based histopathology was 91.1% based on the results of CK19 immunohistochemistry–based histopathology. The sensitivities of the one- and two-level CK19

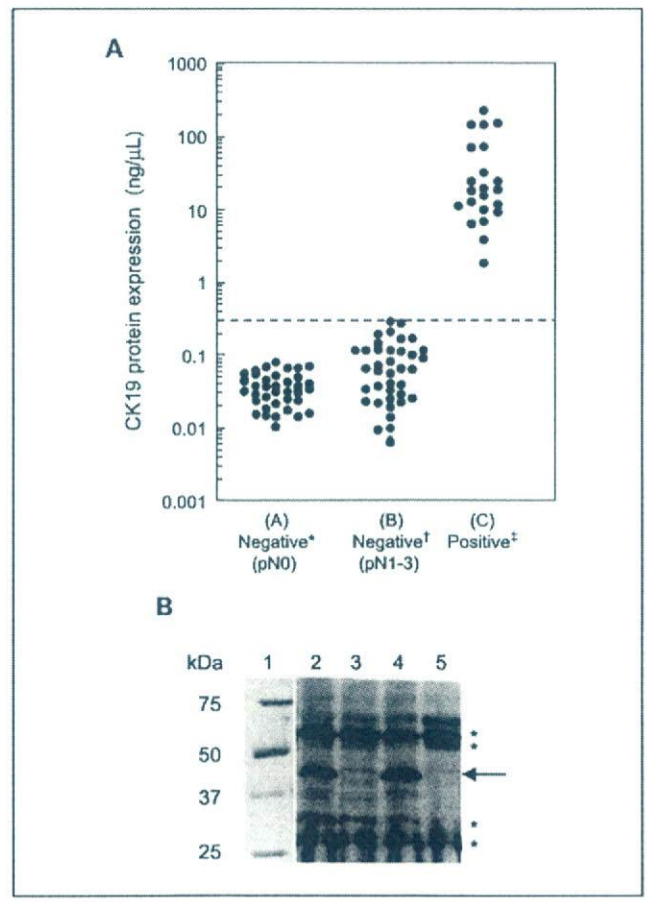

Fig. 5. CK19 protein expression in lymph node lysates. *A*, CK19 protein expression in histopathologically positive and negative lymph node lysates. *, histopathologically negative lymph nodes dissected from pN0 patients. †, histopathologically negative lymph nodes dissected from pN1-3 patients. ‡, histopathologically positive lymph nodes. The CK19 protein expression was determined by Western blot analysis (see Materials and Methods). Broken line, cutoff line between micrometastasis and nonmetastasis. The protein concentration of representative lymph node lysates used in this experiment was within the range of 8.7 to 11.6 μg/μL. *B*, a representative example of Western blot analysis of CK19 protein in lymph node lysates. Lane 1, molecular weight markers stained with Coomassie brilliant blue. Lanes 2 and 4, histopathologically positive lymph node lysate. Lanes 3 and 5, histopathologically negative lymph node lysate. Arrow, CK19 protein. *, nonspecific bands. The vertical scale shows molecular weights.

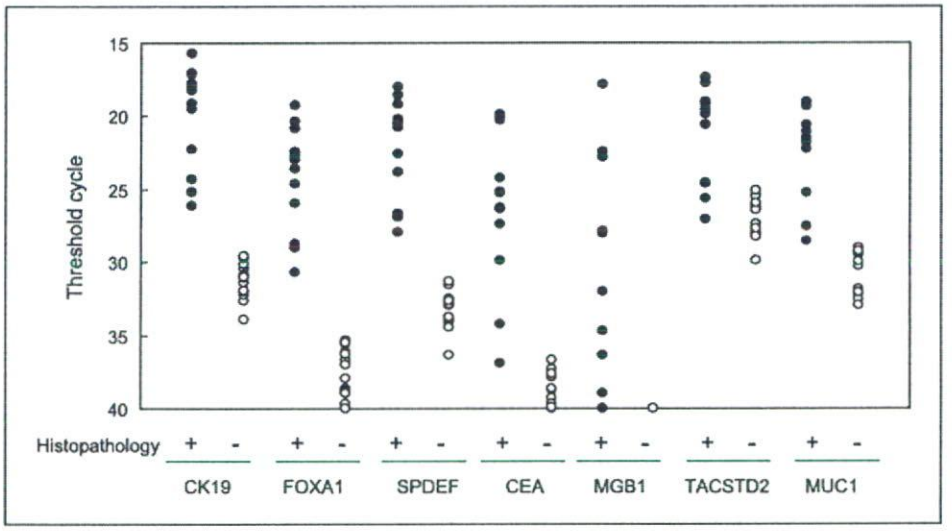

Fig. 6. Expression of mRNA markers in histopathologically positive and negative lymph nodes. The selected mRNA markers (CK19, FOXA1, SPDEF, CEA, MGB1, TACSTD2, and MUC1) were evaluated by QRT-PCR using 11 histopathologically positive (●) and 15 negative (○) lymph nodes from 26 patients.

immunohistochemistry-based histopathologies were 86.7% and 91.1%, respectively, based on the results of three-level CK19 immunohistochemistry-based histopathology (Supplementary Table S3).

The concordance rate between the OSNA assay and the CK19 immunohistochemistry-based three-level histopathology for 325 lymph nodes was 98.2%. The concordance rate for SLNs was 96.4%.

No false positive results were found with the OSNA assay of 144 histopathologically negative lymph nodes from 60 pN0 patients, in which neither micrometastasis nor macrometastasis was observed for serial sections from blocks b′ and d′ (Fig. 3C). Furthermore, the OSNA assay judged 13 ITC cases as negative. These results are summarized in Table 3.

Discordant cases. Six discordant cases were observed between the OSNA assay and CK19 immunohistochemistry-based histopathologic examination (Table 4). Four cases were micrometastasis according to the OSNA assay and were negative according to the CK19 immunohistochemistry-based histopathology. In any case, CK19 mRNA expression of $>10^3$ copies/μL was observed (Table 4). These four discordant cases came from pN1 and pN2 patients. In two of four cases, micrometastasis was observed in the multilevel examinations of blocks b′ and d′. On the other hand, two remaining cases (Table 4, *samples 5* and *6*) were negative according to the OSNA assay and micrometastasis according to the three-level histopathology. Samples 5 and 6 showed metastatic foci of 0.3 and 0.4 mm in the long axis, which were observed on surfaces i′ and ii′, respectively. When i′ and ii′ were histopathologically examined, about 0.2 mm was shaved from the surfaces of blocks b′ and d′. Therefore, the amount of metastatic foci in blocks a′ and c′ that were used for the OSNA assay (i.e., a′ and c′) could not be quantified.

We also measured the amount of CK19 protein by Western blot analysis of the lysate used in each discordance case. A cutoff value for CK19 protein expression between metastasis positive and negative lymph node was determined by the distribution of CK19 protein expression in 37 histopathologically negative lymph nodes from 16 pN0 patients. The distribution could be described as a logarithmic normal distribution. The statistical analysis indicated that an average value +3 SD was 0.13 ng/μL. Based on this analysis, the cutoff value was determined to be 0.3 ng/μL, which is the upper limit of the CK19 protein expression in 54 histopathologically negative lymph nodes from pN1-3 patients (Fig. 5A). Furthermore, CK19 protein expression in 22 histopathologically positive lymph nodes from 10 patients contained protein levels over the cutoff value.

Based on this cutoff value, we measured the amount of CK19 protein using quantitative Western blot analysis of the lysate for the OSNA assay of samples 1, 2, and 5. As described in Table 4, samples 1 and 2 showed an amount of CK19 protein expression equivalent to micrometastasis. Sample 5 exhibited no CK19 protein expression.

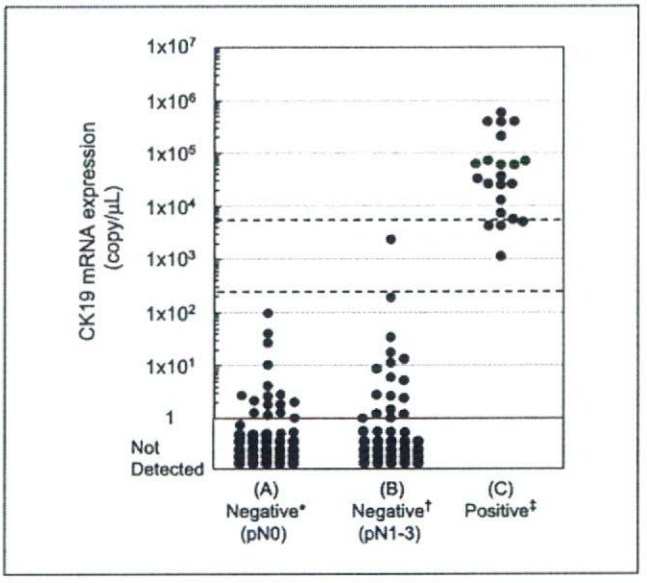

Fig. 7. CK19 mRNA expression in the OSNA assay carried out under the protocol A (Fig. 3 A). *, histopathologically negative lymph nodes dissected from pN0 patients. †, histopathologically negative lymph nodes dissected from pN1-3 patients. ‡, histopathologically positive lymph nodes. Top broken line, cutoff between macrometastasis and micrometastasis. Bottom broken line, cutoff between micrometastasis and nonmetastasis.

Table 3. Comparison of the OSNA assay with the histopathologic examination

Number of lymph nodes	OSNA*	Histopathologic examination †			
		Macrometastasis	Micrometastasis	ITC	Negative ‡
325 from 101 patients	++	34 (34)	0 (0)	0 (0)	0 (0)
	+	6 (5)	3 (1)	0 (0)	4 (0)
	-	0 (0)	2 (2)	13 (11)	263 (0)
81 SLNs from 49 patients	++	11 (11)	0 (0)	0 (0)	0 (0)
	+	1 (0)	2 (1)	0 (0)	1 (0)
	-	0 (0)	2 (2)	3 (2)	61 (0)
144 from 60 pN0 patients	++	0 (0)	0 (0)	0 (0)	0 (0)
	+	0 (0)	0 (0)	0 (0)	0 (0)
	-	0 (0)	0 (0)	3 (3)	141 (0)

*In the OSNA assay, (++), (+), and (-) show >5 × 10^3, 2.5 × 10^2 to 5 × 10^3, and <2.5 × 10^2 copies/μL of CK19 mRNA, respectively.
† Histopathologic examinations with H&E and CK19 immunohistochemistry were carried out in all samples. In cases where metastatic foci were observed in the histopathologic examination by either H&E or CK19 immunohistochemistry, the sample was categorized as macrometastasis, micrometastasis, or ITC. The results of the three-level CK19 immunohistochemistry–based histopathologic examination were determined by the consensus of three third-party pathologists. The number of lymph nodes judged to be positive based on the three-level H&E-based histopathologic examination is shown in parenthesis.
‡ No cancer cells were observed in either the immunohistochemistry- or H&E-based histopathologic examinations.

Discussion

The detection of lymph node metastasis by RT-PCR (37–40) and by QRT-PCR (12, 19–25) has been studied previously. CK19 mRNA has been described as having the highest sensitivity at nearly 90%. However, there are drawbacks using CK19 mRNA due to the concomitant amplification of pseudogenes in genomic DNA that lead to false positive results. For this reason, a combination of two or three markers has been used.

We evaluated 45 potential mRNAs and finally selected CK19 mRNA as the best marker for the OSNA assay. To use CK19 mRNA as a marker, we designed RT-LAMP primers that do not amplify the known CK19 pseudogenes (see Materials and Methods). In addition, the lymph node solubilization step in the OSNA assay was carried out at pH 3.5. At this pH, almost all genomic DNA precipitates out. Even when the sample still contained genomic DNA, DNA amplification is unlikely to occur in the OSNA assay because the RT-LAMP step is carried out at 65°C, a temperature at which genomic DNA typically does not denature. Indeed, purified genomic DNA from metastatic lymph nodes was not amplified in the OSNA assay.

In the present clinical study assessing 325 lymph nodes from 101 patients, an overall concordance rate between the OSNA assay and the CK19 immunohistochemistry–based three-level histopathology was 98.2%. A concordance rate of 96.4% was obtained with 81 SLNs from 49 patients. On the other hand, 1 of 40 macrometastatic cases and 2 of 5 micrometastatic lymph nodes, as defined by CK19 immunohistochemistry–based histopathology, were missed by H&E-based histopathology. Therefore, the sensitivity of three-level H&E-based histopathology was 93.3% based on the three-level CK19 immunohistochemistry–based histopathology. Furthermore, the sensitivity of one- and two-level CK19 immunohistochemistry–based histopathologies is 86.7% and 91.1%, respectively, based on the three-level CK19 immunohistochemistry–based histopathology (Supplementary Table S3). These results indicate that the performance of the OSNA assay is better than that of one- and two-level CK19 immunohistochemistry–based histopathologies and almost equivalent to three-level CK19 immunohistochemistry–based histopathology.

Chu and Wiess (41) reported that 98.2% of primary breast cancer tissues exhibit CK19 protein expression. Two of our authors (Tsujimoto and Tsuda) also examined the CK19 immunohistochemistry–based histopathologic examination of primary breast cancer tissues and found that there was no CK19 protein expression in 20 (2.2%) of 896 cases examined. However, low CK19 mRNA expression in lymph nodes has not been reported.

Table 4. Discordant cases between the OSNA assay and three-level histopathologic examination

Discordant case	CK19 mRNA (copy/μL)	CK19 protein (ng/μL)*	Histopathologic examination †	Nodal status
1	9.6 × 10^2	1.4	Negative	pN2
2	1.5 × 10^3	1.6	Negative	pN1
3	2.3 × 10^3	Not tested	Negative	pN1
4	3.6 × 10^3	Not tested	Negative	pN1
5	ND	0.04	Micrometastasis	pN1
6	ND	Not tested	Micrometastasis	pN1

Abbreviation: ND, not detected.
*Amount of CK19 protein was determined by Western blot analysis (see Materials and Methods).
† Results of CK19 immunohistochemistry–based histopathologic examination of the sections i', ii', and iii' of protocol C (Fig. 3C).

In the present clinical study, CK19 immunohistochemistry–based histopathologic examination of two lymph nodes from one patient revealed metastatic foci smaller than macrometastasis despite the presence of macrometastasis defined by H&E-based histopathologic examination; the histologic type of this primary tumor was neuroendocrine carcinoma. These samples unequivocally had low CK19 expression. The OSNA assay of these samples was positive, indicating that CK19 mRNA was expressed despite the low protein expression found by CK19 immunohistochemistry.

In QRT-PCR studies in which several mRNA markers have been used (12, 19, 24, 25), the ability to quantitatively discriminate macrometastasis from micrometastasis has not been discussed. In the OSNA assay, the solubilization of a lymph node is followed by mRNA amplification. Regardless of the size of the lymph node, a constant portion of lysate is transferred to an RT-LAMP reaction. This indicates that the OSNA assay can, in principle, discriminate macrometastasis from micrometastasis and micrometastasis from nonmetastasis when the cutoff values of CK19 mRNA are properly set. To ensure the quantitative capacity of the OSNA assay, endogenous factors should not interfere with the RT-LAMP reaction. We showed that the presence of a lysate obtained from a lymph node (130-600 mg) did not interfere with the OSNA assay (Fig. 1B). A 600-mg sample of lymph node is equivalent to that having a diameter of about 1 cm. The presence of fat or the reagents that were used to identify SLNs, e.g., radioisotope colloid and blue dyes, did not also interfere with the reaction (data not shown).

We observed no false positive result in the OSNA assay from 144 histopathologically negative lymph nodes (60 pN0 patients). In the statistical analysis of the copy numbers of CK19 mRNA in these 144 lymph nodes, the average value of CK19 mRNA expression +3 SD was $<2.5 \times 10^2$ copies/μL, indicating that the probability of negative lymph nodes showing $>2.5 \times 10^2$ copies/μL is low in the OSNA assay. In the OSNA assay, all 13 ITC cases were judged as nonmetastasis (Table 3).

Based on the serial sectioning experiment (Table 1), the average copy numbers equivalent to 0.2^3, 0.3^3, and 0.4^3 mm^3 can be calculated to be 3.9×10^1, 1.3×10^2, and 3.1×10^2 copies/μL, respectively. Therefore, the cutoff value of 2.5×10^2 copies/μL in the OSNA assay can theoretically detect metastatic foci of 0.3^3 to 0.4^3 mm^3.

The OSNA assay identified 34 cases of macrometastasis out of 40 macrometastatic lymph nodes defined by the permanent three-level CK19 immunohistochemistry–based histopathology. The concordance rate was 85.0%. The remaining six cases were identified as micrometastasis. This is the first example of a molecular biological method with the potential to quantify the size of metastatic foci in a lymph node.

Six discordant cases were observed between the OSNA assay and CK19 immunohistochemistry–based histopathologic examination (Table 4). The quantitative Western blot analysis of the discordant cases (samples 1 and 2) clearly showed the presence of an amount of CK19 protein equivalent to micrometastasis. Although the possible presence of benign epithelial cells such as glandular inclusions in the lymph nodes cannot be eliminated, the results may be better explained by the presence of metastatic foci in the lymph nodes in light of the results of the specificity study and the amount of CK19 protein expression. Two other cases (Table 4, *samples 5* and 6) were negative according to the OSNA assay, but were judged positive for micrometastasis according to three-level histopathology. These two cases showed metastatic foci of 0.3 and 0.4 mm. Therefore, the amount of metastatic foci in blocks a′ and c′ used for the OSNA assay cannot be estimated exactly. Indeed, in sample 5, the quantitative Western blot analysis of CK19 protein showed no expression of CK19 protein (Table 4).

The results of the clinical study indicate that using one-half of a lymph node in the OSNA assay gave nearly the same results as the three-level histopathology. It became clear in the clinical study conducted at six facilities that the OSNA assay is rapid enough to be done during surgery. Furthermore, the assay would be convenient and objective compared with the intraoperative immunohistochemistry-based histopathologic examination, which is usually done by an experienced pathologist (42, 43).

Acknowledgments

We thank Dr. T. Notomi (Eiken Chemical, Japan) for providing the CK19 cDNA, Dr. Masashi Takeda (National Hospital Organization Osaka National Hospital), Dr. Kenichi Wakasa (Osaka City University Medical School), and Dr. Tsuyoshi Okino (Osaka Sailor Hospital) for conducting the histopathology as third-party pathologists, and Dr. Satoshi Teramukai (Kyoto University) for managing the clinical information. We also thank the staff of the clinical and pathologic laboratories at each facility for their support. Thanks also go to Yoshihito Yamamoto, Yasumasa Akai, Katsuhito Matsumoto, Masahiro Nishida, Dr. Junyi Ding, Dr. Hideki Takata, and Kayo Hiyama for supporting the construction of the OSNA assay system. Finally, we express special thanks to Dr. Tameo Iwasaki, Sysmex Corporation, for his helpful advice and encouragement.

References

1. Donegan WL. Tumor-related prognostic factors for breast cancer. CA Cancer J Clin 1997;47:28–51.
2. van Diest PJ, Peterse HL, Borgstein PJ, Hoekstra O, Meijer CJ. Pathological investigation of sentinel lymph nodes. Eur J Nucl Med 1999;26:S43–9.
3. Weaver DL, Krag DN, Ashikaga T, Harlow SP, O'Connell M. Pathologic analysis of sentinel and nonsentinel lymph nodes in breast carcinoma: a multicenter study. Cancer 2000;88:1099–107.
4. Sabel MS, Zhang P, Bamwell JM, Winston JS, Hurd TC, Edge SB. Accuracy of sentinel node biopsy in predicting nodal status in patients with breast carcinoma. J Surg Oncol 2001;77:243–6.
5. Stitzenberg KB, Calvo BF, Iacocca MV, et al. Cytokeratin immunohistochemical validation of the sentinel node hypothesis in patients with breast cancer. Am J Clin Pathol 2002;117:729–37.
6. Luini A, Gatti G, Ballardini B, et al. Development of axillary surgery in breast cancer. Ann Oncol 2005;16:259–62.
7. Cote RJ, Peterson HF, Chaiwun B, et al. Role of immunohistochemical detection of lymph-node metastases in management of breast cancer. International Breast Cancer Study Group. Lancet 1999;354:896–900.
8. Van Diest PJ, Torrenga H, Borgstein PJ, et al. Reliability of intraoperative frozen section and imprint cytological investigation of sentinel lymph nodes in breast cancer. Histopathology 1999;35:14–8.
9. Torrenga H, Rahusen FD, Meijer S, Borgstein PJ, van Diest PJ. Sentinel node investigation in breast cancer: detailed analysis of the yield from step sectioning and immunohistochemistry. J Clin Pathol 2001;54:550–2.
10. Lyman GH, Giuliano AE, Somerfield MR, et al. American Society of Clinical Oncology guideline recommendations for sentinel lymph node biopsy in early-stage breast cancer. J Clin Oncol 2005;23:7703–20.
11. Tanis PJ, Boom RP, Koops HS, et al. Frozen section investigation of the sentinel node in malignant melanoma and breast cancer. Ann Surg Oncol 2001;8:222–6.
12. Hughes SJ, Xi L, Raja S, et al. A rapid, fully automated, molecular-based assay accurately analyzes sentinel lymph nodes for the presence of metastatic breast cancer. Ann Surg 2006;243:389–98.
13. Leidenius MH, Krogerus LA, Toivonen TS, Von Smitten KJ. The feasibility of intraoperative diagnosis of sentinel lymph node metastases in breast cancer. J Surg Oncol 2003;84:68–73.
14. Fortunato L, Amini M, Frrina M, et al. Intraoperative

examination of sentinel nodes in breast cancer: is the lass half full or half empty? Ann Surg Oncol 2004;11: 1005–10.

15. Pugliese MS, Kohr JR, Allison KH, Wang NP, Tickman RJ, Beatty JD. Accuracy of intraoperative imprint cytology of sentinel lymph nodes in breast cancer. Am J Surg 2006;192:516–9.
16. Caemon M, Olsha O, Rivkin L, Spira RM, Golomb E. Intraoperative palpation for clinically suspicious axillary sentinel lymph nodes reduces the false-negative rate of sentinel lymph node biopsy in breast cancer. Breast J 2006;12:199–201.
17. Salem AA, Douglas-Jones AG, Sweetland HM, Mansel RE. Intraoperative evaluation of axillary sentinel lymph nodes using touch imprint cytology and immunohistochemistry. Part II. Results. Eur J Surg Oncol 2006;32:484–7.
18. Brogi E, Torres-Matundan E, Tan LK, Cody HS III. The results of frozen section, touch preparation, and cytological smear are comparable for intraoperative examination of sentinel lymph nodes: a study in 123 breast cancer patients. Ann Surg Oncol 2005;12:173–80.
19. Mitas M, Mikhitarian K, Walters C, et al. Quantitative real-time RT-PCR detection of breast cancer micrometastasis using a multigene marker panel. Int J Cancer 2001;93:162–71.
20. Inokuchi M, Ninomiya I, Tsugawa K, Terada I, Miwa K. Quantitative evaluation of metastases in axillary lymph nodes of breast cancer. Br J Cancer 2003;89: 1750–6.
21. Weigelt B, Bosma AJ, Hart AA, Rodenhuis S, van 't Veer LJ. Marker genes for circulating tumour cells predict survival in metastasized breast cancer patients. Br J Cancer 2003;88:1091–4.
22. Weigelt B, Verduijn P, Bosma AJ, Rutgers EJ, Peterse HL, van't Veer LJ. Detection of metastases in sentinel lymph nodes of breast cancer patients by multiple mRNA markers. Br J Cancer 2004;90:1531–7.
23. Sakaguchi M, Virmani A, Dudak MW, et al. Clinical relevance of reverse transcriptase-polymerase chain reaction for the detection of axillary lymph node metastases in breast cancer. Ann Surg Oncol 2003;10: 117–25.
24. Backus J, Laughlin T, Wang Y, et al. Identification and characterization of optimal gene expression markers for detection of breast cancer metastasis. J Mol Diagn 2005;7:327–36.
25. Nissan A, Jager D, Roystacher M, et al. Multimarker RT-PCR assay for the detection of minimal residual disease in sentinel lymph nodes of breast cancer patients. Br J Cancer 2006;94:681–5.
26. Notomi T, Okayama H, Masubuchi H, et al. Loop-mediated isothermal amplification of DNA. Nucleic Acids Res 2000;28:E63.
27. Nagamine K, Hase T, Notomi T. Accelerated reaction by loop-mediated isothermal amplification using loop primers. Mol Cell Probes 2002;16:223–9.
28. Parida M, Posadas G, Inoue S, Hasebe F, Morita K. Real-time reverse transcription loop-mediated isothermal amplification for rapid detection of West Nile virus. J Clin Microbiol 2004;42:257–63.
29. Yoshikawa T, Ihira M, Akimoto S, et al. Detection of human herpesvirus 7 DNA by loop-mediated isothermal amplification. J Clin Microbiol 2004;42:1348–52.
30. Hong TC, Mai QL, Cuong DV, et al. Development and evaluation of a novel loop-mediated isothermal amplification method for rapid detection of severe acute respiratory syndrome coronavirus. J Clin Microbiol 2004;42:1956–61.
31. Poon LL, Leung CS, Tashiro M, et al. Rapid detection of the severe acute respiratory syndrome (SARS) coronavirus by a loop-mediated isothermal amplification assay. Clin Chem 2004;50:1050–2.
32. Fukuda S, Takao S, Kuwayama M, Shimazu Y, Miyazaki K. Rapid detection of norovirus from fecal specimens by real-time reverse transcription-loop–mediated isothermal amplification assay. J Clin Microbiol 2006;44:1376–81.
33. Schmitt AO, Specht T, Beckmann G, et al. Exhaustive mining of EST libraries for genes differentially expressed in normal and tumour tissues. Nucleic Acids Res 1999;27:4251–60.
34. Mori Y, Nagamine K, Tomita N, et al. Detection of loop-mediated isothermal amplification reaction by turbidity derived from magnesium pyrophosphate formation. Biochem Biophys Res Commun 2001; 289:150–4.
35. Mori Y, Kitao M, Tomita N, et al. Real-time turbidimetry of LAMP reaction for quantifying template DNA. J Biochem Biophys Methods 2004; 59:145–57.
36. Gusterson BA. The new TNM classification and micrometastases. Breast 2003;12:387–90.
37. Min CJ, Tafra L, Verbanac KM. Identification of superior markers for polymerase chain reaction detection of breast cancer metastases in sentinel lymph nodes. Cancer Res 1998;58:4581–4.
38. Manzotti M, Dell'Orto P, Maisonneuve P, Zurrida S, Mazzarol G, Viale G. Reverse transcription-polymerase chain reaction assay for multiple mRNA markers in the detection of breast cancer metastases in sentinel lymph nodes. Int J Cancer 2001;95: 307–12.
39. Noguchi S, Aihara T, Nakamori S, et al. The detection of breast carcinoma micrometastases in axillary lymph nodes by means of reverse transcriptase-polymerase chain reaction. Cancer 1994;74: 1595–600.
40. Bostick PJ, Huynh KT, Sarantou T, et al. Detection of metastases in sentinel lymph nodes of breast cancer patients by multiple-marker RT-PCR. Int J Cancer 1998;79:645–51.
41. Chu PG, Wiess LM. Keratin expression in human tissues and neoplasms. Histopathology 2002;40: 403–39.
42. Lee IK, Lee HD, Jeong J, et al. Intraoperative examination of sentinel lymph nodes by immunohistochemical staining in patients with breast cancer. Eur J Surg Oncol 2006;32:405–9.
43. Nahrig JM, Richter T, Kuhn W, et al. Intraoperative examination of sentinel lymph nodes by ultrarapid immunohistochemistry. Breast J 2003;9: 277–81.